15

NASA
Technical
Paper
2684

January 1987

# Large-Scale Static Investigation of Circulation-Control-Wing Concepts Applied to Upper-Surface-Blowing Aircraft

M. D. Shovlin,
R. J. Englar,
J. C. Eppel, and
J. H. Nichols, Jr.

NASA

**NASA Technical Paper 2684**

1987

# Large-Scale Static Investigation of Circulation-Control-Wing Concepts Applied to Upper-Surface-Blowing Aircraft

M. D. Shovlin
*Ames Research Center*
*Moffett Field, California*

R. J. Englar
*David Taylor Naval Ship Research and Development Center*
*Bethesda, Maryland*

J. C. Eppel
*Ames Research Center*
*Moffett Field, California*

J. H. Nichols, Jr.
*David Taylor Naval Ship Research and Development Center*
*Bethesda, Maryland*

NASA
National Aeronautics and Space Administration

**Scientific and Technical Information Branch**

SYMBOLS

| | |
|---|---|
| $A_j$ | CCW-slot exit area, $in.^2$ |
| $A_{noz}$ | engine-nozzle exhaust area, $in.^2$ |
| $a_j$ | speed of sound in CCW slot exit, ft/sec |
| $b_j$ | nozzle slot span, in. |
| c | airfoil chord, in. |
| $C_u$ | $\frac{\dot{m}V_j}{A_j q}$ |
| F | calculated or measured force, lb |
| $G_{fuel}$ | fuel volume used, gal |
| g | acceleration due to gravity, $ft/sec^2$ |
| $h_{nom}$ | nominal unpressurized CCW slot height, in. |
| $h_j$ | pressurized CCW slot height, in. |
| I | initial force or loading measured at load pad, lb |
| $K_a, K_b$ | balance temperature sensitivities, 1°F |
| $K_x, K_z$ | first-order balance sensitivities, 1/lb |
| $K_{x,z}, K_{z,x}$ | second-order linear balance sensitivities, 1/lb |
| $K_{x,xz}, K_{z,xz}$ | second-order nonlinear balance sensitivities, 1/lb |
| L | measured load or force at each load pad |
| $\dot{m}$ | $\frac{\dot{w}}{g}$ slot-mass flow rate, slugs/sec |
| mv | strain-gage balance output, V |
| $N_1$ | fan speed |
| P | pressure, $lb/in.^2$ |
| $P_{ref}$ | standard day atmospheric pressure, $lb/in.^2$ |

| | |
|---|---|
| $R$ | universal gas constant; $R_{air}$ = 53.3 ft-lb/lb°R |
| $r$ | CCW coanda surface radius, in. |
| $T$ | temperature, °F |
| $T_{ref}$ | standard day atmospheric temperature, °F |
| $t_c$ | calibration temperature of flexure beam, °F |
| $t_1$ | balance temperature at static measurement, °F |
| $T_{installed}$ | installed engine thrust, including flap, nozzle, nacelle, and vortex-generator losses, lb |
| $T_{resultant}$ | resolved engine thrust after turning, lb |
| $t_2$ | balance temperature during load measurement, °F |
| $V$ | velocity, ft/sec |
| $v$ | balance excitation voltage, V |
| $W_{fuel}$ | weight of fuel, lb |
| $\dot{w}$ | slot-weight flow rate; (m)(g); lb/sec |
| $\delta_{USB}$ | USB-flap deflection angle, deg |
| $\theta_R$ | resultant force angle (see fig. 18), deg |
| $\theta_W$ | wind angle to aircraft body axis, deg |
| $\rho_{fuel}$ | fuel density, lb/gal |
| $\gamma$ | $\frac{C_p}{C_v}$ ; ratio of specific heats. For air at standard condition $\gamma$ = 1.4 |

Subscripts:

| | |
|---|---|
| a | air |
| d | duct; CCW plenum; total pressure or temperature |
| i | 1,2,3; station location (see fig. 18) |
| j | jet |

| | |
|---|---|
| R | resultant |
| W | wind |
| X | horizontal |
| Z | vertical |
| $\infty$ | free stream, ambient |

# LARGE-SCALE STATIC INVESTIGATION OF CIRCULATION-CONTROL-WING CONCEPTS APPLIED TO UPPER-SURFACE-BLOWING AIRCRAFT

M. D. Shovlin, R. J. Englar,* J. C. Eppel, and J. H. Nichols, Jr.*

Ames Research Center

## ABSTRACT

The use of a circulation control to deflect turbofan engine thrust beyond 90° has been proven in full-scale static ground tests of the circulation-control-wing/upper-surface-blowing (CCW/USB) concept. This powered high-lift system employs a circular, blown trailing edge to replace the USB mechanical flaps to entrain engine-exhaust flow, and to obtain both a vertical-thrust component and an augmented circulation lift for short takeoff and landing (STOL) applications. Previous tests (Phase I), done in 1982, of a basic configuration installed on the Quiet Short Haul Research Aircraft confirmed these CCW/USB systems capabilities. A second phase (Phase II) of full-scale, static, thrust-deflection investigations has reconfirmed the ability to deflect engine thrust from 40° to 102°, depending on thrust level. Five new configurations were evaluated and performance improvements were noted for those configurations with larger blown span, fences or favorable engine interactions, smaller slot height, and larger radii with less than 180° of CCW surface arc. In general, a 90° circular arc with a smaller slot height provided the best performance, demonstrating that adequate thrust turning can be produced by a trailing-edge shape which may have minimal cruise-performance penalty. Thrust deflections were achieved at considerably lower blowing momentum than was required for the baseline case of Phase I. Improved performance and versatility were thus confirmed for the CCW/USB system applied to STOL aircraft, where the potential for developing a no-moving-parts pneumatic thrust deflector to rapidly vary horizontal force from thrust to drag, while maintaining constant vertical force, appears quite promising. The conversion from high-lift to lower-drag cruise mode by merely terminating the blowing provides an effective STOL aircraft system.

## INTRODUCTION

The requirements for improved lifting, maneuver capability, and short takeoff and landing (STOL) characteristics, for both military and civil aircraft, have led to the development of several technology demonstrator aircraft to perform research in powered-lift aerodynamics. Two of these, NASA's Quiet Short-Haul Research

*Aircraft Division, David Taylor Naval Ship Research and Development Center, Bethesda, Maryland.

Aircraft (QSRA), and the Navy/Grumman A-6/Circulation-Control-Wing Flight-Demonstration Aircraft (figs. 1 and 2), have provided extensive data for the upper-surface-blowing (USB) and circulation-control-wing (CCW) concepts of powered-lift. A powered-lift concept (fig. 3 and refs. 1-4) developed at the David Taylor Naval Ship Research and Development Center (DTNSRDC) replaces the mechanical flap system of the USB airplane with a CCW flap which deflects the engine thrust. The resulting increase in wing circulation and the vertical-thrust component greatly augments aerodynamic lift in a manner similar to that of the USB flap concept used in the QSRA and the Air Force/Boeing YC-14 airplanes.

The ability of this CCW/USB configuration to deflect engine thrust to angles greater than 90° was verified in a full-scale static ground test conducted on the QSRA in 1981 (ref. 5). This investigation (referred to as Phase I) was undertaken to confirm that full-scale, static-thrust deflection could be accomplished by the CCW/USB concept; to compare that thrust turning to model-scale results; and to identify any problems produced by the mixed-flow exhaust of a turbofan engine. A second test series, Phase II, was planned to investigate CCW/USB geometry which would be more representative of a flight configuration.

During the Phase I investigation, the potential for a full-scale CCW/USB system was demonstrated with thrust turning, ranging from 97° to 40°, depending upon the thrust level. However, the blowing momentum required for thrust-angle change, based on the model-scale data in reference 3, was higher than expected. Two probable causes for this reduced performance were determined during the investigation. The first of these was the CCW trailing-edge design, which permitted distortion and deflection in the jet-nozzle upper lip with increasing jet temperature and pressure. As noted in reference 6, large slot heights at high jet pressures can lead to serious deficiencies in performance. The second cause for reduced performance resulted from a substantial amount of engine flow being spread beyond the physical limits of the CCW trailing edge, and, therefore, not being turned. During normal operation, an interference between inboard and outboard engine exhausts causes the flow to be channeled over the flap directly behind the engine. When only one engine is operated, as was done during these tests, the exhaust flow is mechanically spread beyond the flap to improve the aircraft's engine-out performance (ref. 7).

Thus, aside from confirming the potential of the CCW/USB system for STOL application, these Phase I investigations suggested some improvements that should be evaluated to increase overall system effectiveness. Among the improvements suggested were

1. Reduce the thickness of the CCW thrust-deflecting surface to decrease blowing-off cruise drag.

2. Design additional CCW trailing-edge configurations which improve upon the full circular trailing edge of Phase I, in which the average trailing-edge radius/chord ratio was 0.0362.

3. Increase the blown system span to ensure that portions of the jet exhaust spread by the D-nozzle and vortex generators were being turned.

4. Increase the available blowing supply pressure and momentum to extend the range of flow turning available.

5. Evaluate the effect of variation in blowing slot height.

A second series (Phase II) of joint NASA/Navy static ground tests was conducted in August 1983 with CCW design incorporating the suggested improvements. Two reduced-thickness CCW trailing edges were designed by DTNSRDC and constructed by Micro Craft, Inc. of Tullahoma, Tennessee. These configurations were then installed, instrumented, and tested behind the left inboard engine of the QSRA, as was done in the Phase I tests. The results of this investigation are presented in the following sections.

## AIRPLANE DESCRIPTION

The QSRA is shown in figure 1, and the aircraft's general configuration is shown in figure 4. The fuselage is a de Havilland C-8A Buffalo with structural reinforcements in the aft section, and new fairings at the wing-body intersection. The C-8A empennage was used without structural or aerodynamic modification, but the landing gear was modified to increase the sink-rate capability of the aircraft.

The QSRA wing, designed and fabricated by Boeing, has a wingspan of 73.5 ft, a wing area of 600 $ft^2$, and quarter chord sweep of 15°. The fixed, leading-edge flaps are slotted to provide boundary-layer control aerodynamically. The trailing edge on either side of the centerline consists of two USB flaps, a double-slotted flap, and a drooped, blown aileron. Additional aircraft descriptive information is contained in reference 8.

## PROPULSION SYSTEM

The QSRA propulsion system consists of four AVCO-Lycoming YF-102(QSRA) engines mounted in above-the-wing nacelles. These prototype engines, acquired from the Air Force A-9A program, are geared fan-jets with a bypass ratio of 6:1; they are similar to the AVCO-Lycoming ALF-502L commercial engine or the General Electric TF-34 engine.

The engine weighs 1,215 lb, and has a basic diameter of 42.4 in. and an overall length of 63.8 in., including the fan spinner; the fan has a diameter of 40.3 in. Although the rated thrust of the engine is 7,500 lb, the standard-day value of installed thrust is about 6,250 lb. Detailed information about the engine performance characteristics and the propulsion system design is given in reference 7.

## Nozzle Design

The exhaust system is a confluent-flow design with both the primary and fan streams discharging through a common, D-shaped exit nozzle with an aspect ratio of 3.5. As indicated in figure 5, the core exhaust diffuses as it passes through the primary nozzle, and then mixes with the surrounding fan stream before exiting through the D-shaped USB nozzle. The core nozzle is canted upward 9.4° relative to the engine centerline to minimize heat effects on the wing.

The flow areas in the fan duct and the core-nozzle exit plane (mixing plane) were sized to provide adequate performance without affecting engine stability. The main control on stability margins and engine-match, however, is provided by the final exit area of the D-nozzle. The exit is designed to spread the exhaust into a thin sheet, which is then turned, in accordance with the Coanda effect, over the USB flaps, thus providing propulsive lift. The efficiency of the jet sheet in providing this propulsive lift is highly dependent on the design and shape of the D-nozzle exit.

For the QSRA, this flow-spreading is enhanced (especially with one engine inoperative) by a cutout that opens toward the adjacent nacelle. Figure 6 shows the cutout in the right inboard engine nozzle. Under normal circumstances, this cutout improves the wing and flow-turning efficiency by inducing a spanwise component of flow and spreading the thin jet sheet over a portion of the adjacent USB flap during engine-out operation.

## Vortex Generators

Two rows of vortex generators are located behind each engine (fig. 6). The forward row was designed to improve the mixing and turning of the primary flow and to energize the boundary layer. The aft row was developed to maximize lift at low angles of attack with an engine inoperative during flight. Although the effect of these vortex generators on the CCW trailing edge is not known, they do increase flow turbulence, especially in the USB-jet boundary layer. This increased turbulence may induce a higher than normal mixing between the USB-jet and CCW-jet sheet, possibly reducing its turning potential.

# CCW TRAILING-EDGE DESIGN

These investigations were intended primarily as a full-scale static proof of concept. Therefore, the test CCW trailing edges were designed as simple bolt-on configurations installed behind the left inboard QSRA engine. As no flight testing was intended, the configurations were not designed to be airworthy and the CCW air supply was provided from external, ground airstart carts instead of from engine bleed air. The CCW devices could not be mounted directly at the trailing edge of the USB flap because the flap-bracket fairings protrude aft of the flap and slightly

above it. Hence, a flat ramp was installed between the USB trailing edge and the CCW trailing edge. The CCW device and ramp were mounted flush with, and tangent to, the USB trailing edge. The CCW trailing edge was externally braced with a strut (fig. 7) which transferred the high lift loads generated by the CCW directly into the left main landing gear and prevented the CCW device from moving relative to the USB flap surface.

## Phase I CCW Design

In the Phase I investigation, Ames Research Center designed, constructed, and installed the CCW device based on parameters supplied by DTNSRDC.

A standard 10-in.-diam tube was used to provide the CCW Coanda surface. This rather large-diameter circular surface was scaled from the trailing edge used in reference 3, and was installed to provide a comparison between full- and model-scale tests. The 75-in. width of the blown trailing edge matched that of the USB flap it was attached to, as shown in figure 8.

## Phase II CCW Design

The Phase II investigation used new CCW configurations provided by DTNSRDC as shown in figure 9. These configurations were designed to investigate reduced trailing-edge thickness and shape variations and the effect of jet height and blowing rate on USB jet-turning efficiency. In addition, the new configurations had increased blown system span and utilized an end plate to more fully entrain the engine exhaust flow.

Trailing-edge design- The basic trailing-edge mounting configuration used in Phase I (fig. 9 in ref. 5) was redesigned to allow interchange of the bolt-on trailing edges. The 90° circular arc configuration had the same 5-in. radius as the circular trailing edge from Phase I, but it produced a trailing-edge projected thickness at the slot location of only slightly over half that of the circular section. It was thus expected to produce about the same thrust turning, but with less cruise drag. The average radius-to-chord ratio (based on a chord tapering from 147.24 in. at the inboard flap station to 126.18 in. at the outboard end of the blow section) was $r/c = 0.03657$. The original circular trailing-edge average $r/c$ was 0.03616, a slightly smaller average value caused by the larger chord at the outboard end ($c = 129.29$ in.). The 90° configuration shown in figure 10 is mounted on a series of brackets attached to the existing flap in its undeflected position. As figure 11 shows, the assembly was located behind the left inboard engine (#2) only, and was attached by a support strut to the left main landing gear to restrain the lifting load on the flap trailing edge.

A second trailing edge, the 5-in.-diam, 180° circular-arc configuration, is shown installed in figure 12. This design was the same as the Phase I circular configuration, but with the radius and thickness halved (average $r/c = 0.01829$).

If the blowing jet flow remained attached to this smaller radius, then thrust turning similar to the 97° achieved during Phase I should be attainable, but with a reduced cruise-drag penalty.

Increased spanwise blowing- In Phase I, the engine exhaust was spread beyond the 75-in. span of the inboard flap by the vortex generators and D-nozzle cutout. In figure 6, the flow patterns on the wing show that the engine exhaust is spread slightly beyond the flap bracket on the adjacent outboard flap. Thus, a portion of the jet exhaust was not exposed to the CCW turning surface. Figure 10 of reference 5 shows that while the tufts at the CCW device were tightly wrapped around the cylinder turning surface, the tuft on the adjacent flap was extended aft of the wing tangent to the flap upper surface. For the present investigation, the CCW trailing edge and slot were lengthened spanwise 13 in. to provide an 88-in. span, which extended the CCW to the first flap bracket on the adjacent USB flap (figs. 11 and 13). A circular fence was mountable at the end of this increased span to further assure that none of the jet was escaping the blown system (fig. 14). On the QSRA, with all engines running, the outboard and inboard exhausts favorably interact to produce this effect, but these tests used only the left inboard engine.

The QSRA's USB flap design also utilizes a similar end-fence concept to prevent free-stream flow from coming in from the side and decreasing the flaps' turning effectiveness. The USB flaps have seals (fig. 11) in the chordwise direction which prevent the flow from leaking between the two USB flaps and seal the flap against the fuselage on the inboard side. On the outboard side, the USB flap seal rides on a fence, which is installed under the double-slotted flap (fig. 14).

CCW air- Three aircraft ground-air-supply carts were used to supply blowing air to the trailing edge; their connectors (fig. 12) were moved farther forward on the lower surface of the assembly to eliminate their interference with the turning exhaust experienced in Phase I. Stronger attachment points for the slot-adjustment screws were provided to prevent slot distortion under pressure. The slot height was reset and measured under pressure and temperature for each new configuration so that its effective slot area could be calculated. After initial runs showed an inboard-upward deflection of the entire CCW assembly caused by the thrust turning, the support rod on the outboard span was augmented by a steel cable inboard to prevent this deflection (fig. 13).

The assembly was instrumented with total pressure and temperature probes to measure conditions inside the blowing plenum chamber and within the jet exhaust stream in the vicinity of the blowing slot (figs. 9, 11, and 12).

## GROUND TEST

### Aircraft Force Measurements

The lift and thrust forces (hence, turning angle) acting on the QSRA were determined by summing the axial and normal forces acting on the landing gear. These

axial and normal forces were measured, using a calibrated strain-gage flexure beam, at each gear station by a load pad. These load pads, originally developed by Boeing for QSRA ground tests, are bolted to steel anchor plates installed on one of the aircraft run-up areas at the Ames V/STOL test site. The main landing gear and nose gear load pads are shown in figure 15, and the aircraft is shown mounted on the load pads in figure 16. The airplane wheels are firmly clamped to a plate mounted on top of the load pads, and the airplane is leveled with respect to the horizontal. Plywood shields are located behind the main gear pads to prevent hot-gas impingement on the load pads during engine operation with high-flow turning angles. The load pads are electrically heated to minimize strain-gage temperature fluctuations and to keep moisture off the flexure beam and the strain-gage terminal strips. The load-pad temperatures and strain-gage excitation voltages were manually recorded before and after each run, and the strain-gage outputs were channeled into the aircraft's flight-data system and recorded continuously. The strain-gage bridges are excited by the regulated power supplies that are built into the aircraft's data system.

## Aircraft Data System

The QSRA is equipped with a high-speed data system composed of transducers, signal-conditioning equipment, a telemetry transmitter, and a tape recorder. This system takes measurements, telemeters data in real time to a ground data facility, and records significant airplane and ground instrumentation parameters for post-test analysis.

Data from the transducers are transmitted to the analog and digital network panels, which provide the necessary signal conditioning. The conditioned data then pass through to the remote multiplexer-digitizer unit (RMDU); the RMDU then adjusts the gains to a programmed level, provides analog-to-digital conversion, and encodes the data in a pulse-code-modulated serial bit stream. The data from the RMDU are recorded on a standard, airborne, 14-track magnetic-tape recorder; they are also telemetered via L-band transmission to a ground station for real-time data monitoring. The aircraft data system contains a time-code generator, which furnishes time correlation for the data. Separate, precision low-voltage power supplies located in the aircraft's analog network panels supply transducer excitation power where required. A more detailed description of system is given in reference 8.

## Meteorological Measurements

The aircraft is equipped with instrumentation that accurately measures atmospheric conditions in flight. However, most of these sensors are of limited use during the ground testing. To have an accurate assessment of the wind-speed and direction, air temperature, humidity, and barometric pressure, a "Met One" weather station (fig. 17) was installed on the test site, located several hundred feet from the aircraft at about wing level. This location was chosen so that the atmospheric readings would be representative of those at the aircraft, but would not be influenced by the aircraft or the ground-support equipment. The meteorological data were

converted to both direct readout and to analog signals by the Met One weather station. The direct readout was used as an aid by test personnel at the site, and the analog signals were channeled into the aircraft data system, giving a continuous record of atmospheric conditions during the test.

## Test Plan

For each configuration and blowing condition, the general plan consisted of advancing the left inboard engine power settings (fan speed) in even 5% increments from ground idle to maximum power and then decreasing the settings in the same manner. Each setting was held for 30 sec before proceeding on to the next condition. A list of the individual test conditions is given in table 1. Static measurements were made before and after each data run to verify data system operation and to provide the tare load history required for analysis.

The CCW trailing edge was installed before the beginning of the test with the 10-in. quarter-round trailing edge and no fence. The nozzle gap was set at a nominal 0.07 in. and the first run was made with no airflow through the nozzle. This test condition set a baseline thrust and turning flow measurement versus fan speed and allowed the CCW trailing edge to heat gradually without being under pressure. For the next run the engine was shut down and the CCW was pressurized with two air carts, with one located at each end of the device. Unlike the CCW trailing edge of Phase I, the nozzle gap had a negligible tendency to grow with temperature and pressure, so the gap could be quickly checked and minor adjustments could be made if required between each new condition. To provide a more even pressure and temperature distribution on the CCW assembly, the following sequence was used for the air-start carts. The first pressurized run was made with the two carts at each end of the CCW device, and a third (center) cart was added for the next test condition. The two end carts were then shut down for the final run, with only the center cart providing air to the CCW device.

## Operational Problems

After a few runs it was noticed that the inboard (unsupported) edge of the CCW assembly was deflecting upward because of the lift forces acting on it. A steel cable was fixed to the CCW inboard end and secured to the main landing gear to solve this problem. Enough tension was applied to the cable to keep the CCW inboard edge from moving in space.

A second problem occurred because of an attempt to alleviate the low resolution of the aircraft data system, particularly at small loads (ref. 5). In the Phase I studies, it was impossible to get meaningful measurements of the CCW turning without the USB engine running. The signal-conditioning cards were modified to allow the use of a high-precision voltmeter to directly measure the analog signals from the strain-gage balances at low- or zero-thrust levels. It was found that the voltmeter affected the output values of the strain-gage balances and, therefore, was not

used. The modifications to the signal-conditioning cards introduced another problem which was a significant zero shift with time. This shift was fairly linear and was confirmed from strip chart recordings taken before and after testing while the airplane was in a static condition. These cards were remodified, and while the zero point shift was not entirely eliminated, it was reduced about two orders of magnitude (i.e., from 50-lb-shift/min to less than 0.5 lb/min). The data were then corrected for these zero shifts based on the time when an individual data point was obtained.

## Baseline Measurement

At the completion of the test series, the CCW assembly was to be removed and the installed-performance evaluation of the left inboard engine was to be obtained as was done in the Phase I studies. However, while the CCW device was being removed, a routine engine inspection indicated the engine fan was not turning freely, and it was decided not to complete the baseline runs.

The baseline performance of Phase I was used for comparison in these studies. A comparison of the performance during Phase I with the similar Phase II performance showed that the resultant thrust over the 10-in. radius trailing edge had decreased from the 98% recovery in Phase I to 95% in Phase II. Based upon the engine records and other data, it is believed that this 3% difference is primarily caused by the degradation of engine performance from increasing age and hot-section hardware changes made to it between the two tests. Therefore, the baseline of Phase I was reduced by 3.1% and was used as the baseline of this test series, giving nearly identical losses over nearly identical CCW hardware (no blowing).

## Real-Time Data Processing

The data were telemetered to the ground station for real-time data processing. The telemetered data stream was decoded, converted to engineering units, and each measured parameter was sampled five times per second. Because of equipment limitations, hard-copy updates of the entire parameter list were obtained only every 4 sec. Real-time processing was used to provide a check of the results to determine the validity of selected parameters that were displayed continuously on strip charts and also on alphanumeric television displays. These parameters included the CCW temperature and pressure; engine speeds, temperatures, and pressures; atmospheric conditions; load-pad axial and normal forces at each landing gear location; and calculated values of the net lift, thrust, flow-turning angle, and CCW-slot jet velocity.

The load-pad force calculations were simplified for real-time processing by accounting for only the first-order linear components from the balances (see Analysis section). The net thrust was calculated by summing the axial forces from the landing-gear load pads. The net lift was obtained in a similar manner from the sum of the load-pad normal forces; however, it had to be corrected for the weight of the

airplane. The weight of the airplane was calculated by subtracting the weight of the fuel used during testing from the initial airplane weight, as recorded by the load pads. The fuel weight was then obtained from the aircraft's fuel totalizers, which recorded the amount of fuel used by each engine. Finally, the resultant thrust was calculated by taking the vector sum of the lift and axial forces; the turning angle was the angle between the resultant and the horizontal forces.

## ANALYSIS

### External Force Measurements

The axial and normal forces at each landing-gear location were measured with a calibrated flexure beam, instrumented with a set of orthogonal strain-gage bridges. The primary effects on these bridge outputs were the level of force, axial or normal, in the direction the bridge was designed to measure, and the value of input excitation voltage to the bridge. Besides these primary effects, several secondary effects also had to be considered to accurately calculate the input loads from the strain-gage outputs. The two most important of these effects are the temperature variation of the flexure beam during the test versus its calibration temperature, and the interaction of axial and normal force through the flexure beam.

### Phase II CCW Design

The current investigation used new CCW configurations provided by DTNSRDC. These configurations were designed to investigate: reduced trailing-edge thickness and shape variation; USB jet turning improvement due to increased blown system span and an end plate to entrain more of the engine exhaust; and the effect of jet height and blowing rate on USB jet turning efficiency. The configurations designed and built to accomplish these goals are shown in figure 9.

Trailing edge design- The basic trailing edge mounting configuration used in Phase I (fig. 9 of ref. 5) was redesigned to allow interchange of the bolt-on trailing edges. The 90° circular arc configuration had the same 5-in. radius as the circular trailing-edge from Phase I, but it produced a trailing edge projected thickness at the slot location of only slightly over half that of the circular section. It was thus expected to produce about the same thrust turning but with less cruise drag. The average radius-to-chord ratio (based on a chord tapering from 147.24 in. at the inboard flap station to 126.18 in. at the outboard end of the blow section) was $r/c = 0.03657$. The original circular trailing-edge average $r/c$ was 0.03616, a slightly smaller average value due to the larger chord at the outboard end ($c = 129.29$ in.). The 90° configuration is shown in figure 10 mounted on a series of brackets attached to the existing flap in its undeflected position. As figure 11 shows, the assembly was located behind only the left inboard engine (#2) and was attached by a support strut to the left main landing gear in order to restrain the lifting load on the flap trailing edge.

## Calculation Procedures

The procedure for determining the load-pad forces consisted of two operations: calculating the initial loads under static conditions and using the outputs of the strain-gage bridges in conjunction with the static loads to determine the actual test axial and normal forces. Since the equations for each load pad are similar (except for different constants), this discussion will show only the procedure for determining the loads from one load pad. Because the load equations contain interaction terms, the normal procedure is to start with a value based on no interactions, and then to iterate the equations, using the previous solution in each successive iteration. This procedure is continued until the difference between iterations is less than 0.005%.

Static load calculation- The static loads are calculated in the following manner.

The initial loads iteration:

$$I_X = \frac{mv_x}{v_X K_x [1 + K_a(t_1 - t_c)]}$$

and

$$I_Z = \frac{mv_Z}{v_Z K_z [1 + K_a(t_1 - t_c)]}$$

Subsequent loads iterations:

$$I_X = \frac{mv_X}{v_X K_x [1 + K_a(t_1 - t_c)]} - \{K_{x,z} I_z + [1 + K_b(t_1 - t_c)] K_{x,xz} I_X I_Z\}$$

and

$$I_Z = \frac{mv_Z}{v_Z K_z [1 + K_a(t_1 - t_c)]} - \{K_{z,x} I_X + [1 + K_b(t_1 - t_c)] K_{z,xz} I_X I_Z\}$$

The intial or static loads are calculated for each data point over a 30-sec period and an average is taken for the entire sample of approximately 150 points. These initial or static loads, along with their average load-pad temperatures and excitation voltages, are recorded for later use in determining the test loads and also in checking the load pads' strain-gage stability.

Test-loads calculation- Once the initial loads have been determined, the balance loads during a test condition are completed in the following manner:

First iterations:

$$L_X = \frac{\Delta mv_X - B_x}{v_X K_x [1 + K_a(t_2 - t_c)]}$$

and

$$L_Z = \frac{\Delta mv_Z - B_Z}{v_Z K_z [1 + K_a(t_2 - t_c)]}$$

where

$$B_X = v_X K_x [K_a(t_2 - t_1)](I_X + K_{x,z} I_Z)$$

and

$$B_Z = v_Z k_z [K_a(t_2 - t_1)](I_Z + K_{z,x} I_X)$$

The terms $\Delta mv_X$ and $\Delta mv_Z$ are defined as the difference between the strain-gage bridge output at the test point and the average of the bridge output during static loading. For the second and subsequent load iterations:

$$L_X = \frac{\Delta mv_X - B_X}{v_X K_x [1 + K_a(t_2 - t_c)]} + K_{x,z} I_Z = [1 + K_b(t_2 - t_c)] K_{x,xz} I_X I_Z$$

$$- K_{x,z}(L_Z + I_Z) - [1 + K_b(t_2 - t_c)] K_{x,xz}(I_X + I_X)(L_Z + I_Z)$$

and

$$L_Z = \frac{\Delta mv_Z - B_Z}{v_X K_x [1 + K_a(t_2 - t_c)]} + K_{z,x} I_X + [1 + K_b(t_2 - t_c)] K_{z,xz} I_X I_Z$$

$$- K_{z,x}(L_X + I_X) - [1 + K_b(t_2 - t_c)] K_{z,xz}(L_X + I_X)(L_Z + I_Z)$$

These forces are calculated for each data point over a 30-sec period and then an average is taken for the entire sample of approximately 150 points. Each test sample is begun only after all of the aircraft and CCW operating parameters have attained a stable condition. Although these aircraft parameters, and hence the loads, are not truly static, the variation is small during the sample period. This procedure of averaging the large number of data points acquired during the sample period has yielded results that are generally repeatable within ±0.05% of the maximum measured forces.

Data system resolution- The data system divides the range of each parameter into 1,024 parts, or counts, to digitally transmit the analog signals from its individual measuring devices. The effect of this digitization is to create discrete

increments of the transmitted value for each parameter that are a constant percentage of its full-scale range. Since the input signal may cover any value in the parameter's range, the incoming signal often will be between discretes or counts, and hence the next higher or lower value will be outputted into the data stream. In the case of the load pads during the current test, this discrete increment was about 50 lb. Averaging a statistically meaningful sample of data tends to minimize the error introduced by these fluctuations, particularly under truly static conditions. Aircraft weight calculations based on load-pad readings were compared with weight readings measured with standard weight scales and were found to correlate within 0.10%.

### Small Loads

Although the load pads and data system give accurate results with large loads, some problems occur when the loading is very low. For the CCW trailing edge alone, the loads are on the order of the data system resolution and the results, during both Phase I and the present studies, do not appear to be consistent from point to point. Hence, no engine-off CCW trailing-edge data have been presented in either study.

## CCW TRAILING-EDGE CALCULATIONS

The individual pressures and temperatures from the CCW plenum and the USB trailing-edge pressure were sampled by the aircraft data system, displayed in real time, and recorded for later processing. These parameters were sampled for 30 sec after they were stabilized on a test condition, at a sample rate of five points per second. The individual plenum temperatures and pressures were averaged for the data analysis.

### CCW-Jet Velocity

The jet velocity was calculated assuming an isentropic expansion from CCW-plenum total conditions to free-stream static conditions:

$$V_j = a_j M_j = (\gamma R g T_j)^{1/2} M_j = \left\{ 2gRT_d \frac{\gamma}{\gamma - 1} \left[ 1 - \left( \frac{P_\infty}{P_d} \right)^{\gamma - 1/\gamma} \right] \right\}^{1/2}$$

It is realized that expansion to local static conditions at the jet exit gives a far more realistic value of $V_j$, and that expansion to free-stream static pressure underestimates $V_j$ and $M_j$. However, local exit conditions are functions of local geometry, and thus a comparison of two blown airfoils of unlike trailing-edge geometry, but of identical slot areas, plenum pressures, and temperatures, would yield

unlike values of momentum coefficient. The momentum coefficient based on expansion to free-stream conditons is thus accepted as a more "universal" parameter for comparison of blown systems.

## CCW-Slot Mass Flow

The mass flow to the CCW slot was provided by a maximum of three aircraft ground-air-supply carts. Because these carts are used daily for aircraft servicing, it was not possible to modify them to accurately measure the mass flow. Hence, the mass flows used in this analysis were calculated for isentropic conditions as follows:

Choked flow:

$$\dot{m}_j = A_j P_d \sqrt{\frac{\gamma}{RgT_d}} \left(\frac{2}{\gamma + 1}\right)^{(\gamma+1)/2(\gamma-1)}, \quad \frac{P_d}{P_\infty} \geq 1.89$$

Unchoked flow:

$$\dot{m}_j = A_j P_d \left\{ \frac{2\gamma}{(\gamma - 1)RgT_d} \left[ \left(\frac{P_\infty}{P_d}\right)^{2/\gamma} - \left(\frac{P_\infty}{P_d}\right)^{\gamma+1/\gamma} \right] \right\}^{1/2}$$

## AIRCRAFT EQUATIONS

The locations and directions of the forces acting on the aircraft are shown in figure 18.

Net axial force- The net axial force is the sum of the axial forces measured by the load pads, corrected for the wind ram drag:

$$F_X = L_{X_1} + L_{X_2} + L_{X_3} + \frac{\dot{w}_a}{g} V_w \cos \theta_w$$

Note: In $\theta_w$ is greater than 90° or less than -90°, then the ram drag term is set equal to zero.

Net lift- The net lift force on the aircraft is the sum of vertical forces as measured by the load pads corrected for the fuel used:

$$F_Z = L_{Z_1} + L_{Z_2} + L_{Z_3} - w_{fuel}$$

where

$$W_{fuel} = G_{fuel} \times \rho_{fuel}$$

Resultant force- The resultant force is

$$F_R = (F_Z^2 + F_X^2)^{1/2}$$

and the resultant angle is

$$\theta_R = \tan^{-1}(F_Z/F_X)$$

Referred parameters- The measured forces and engine parameters are corrected to, or referred to, sea-level, standard-day values to permit direct comparisons with other data from previous tests. The measured forces are corrected by the ratio of ambient barometric pressure to standard-day, sea-level pressure; hence, the referred force = measured force/$(\rho_\infty/P_{ref})$. Similarly, the measured fan speed is corrected by the square root of the ratio of the ambient temperature to standard-day temperature expressed in degrees Kelvin or Rankine:

$$N_{1_{referred}} = N_{1_{measured}} \sqrt{\theta}; \text{ where } \theta = \frac{T_\infty}{T_{ref}}$$

## RESULTS AND DISCUSSION

Data from references 1, 2, 3, and 5 imply that CCW/USB thrust deflection is primarily a function of engine thrust level and CCW-jet characteristics (principally jet pressure and momentum), while references 6 and 9 note that CCW radius and slot height can strongly influence jet turning, especially at higher blowing pressure ratios. These parameters were thus of prime concern in the present investigation. They were varied as shown in table 1 during the program. The configurations tested during Phase II are summarized and compared to the Phase I baseline configuration as shown in table 2.

Thrust deflection- Thrust deflection produced by CCW blowing is shown in figures 19-24 as a function of resultant engine thrust and blowing momentum per unit span, $\dot{m}V_j/b_j$. Resultant thrust shown is the measured static horizontal-vertical force resultant which is experienced during blowing. Although a spanwise component exists, it is not included because there is no side-force component measured on the test-stand load pads. This is of little consequence if one is determining total force on the aircraft with thrust deflected symmetrically on both sides of the fuselage. However, this component can be important for determining thrust-turning efficiency and lateral loads.

Performance improvements are compared to the baseline configuration of Phase I (fig. 24). This baseline trailing-edge configuration is a 10-in.-diam cylinder with approximately 260° of exposed arc downstream of the jet a span equal to the inboard flap on which it is mounted, a slot height which expands under pressure, and no fence. Use of the parameter $\dot{m}V_j/b_j$ (blowing momentum per unit span) allows a direct comparison of the Phase I and II data in terms of momentum expended, even though the physical spans were unequal. Thrust-deflection trends similar to those of Phase I are shown in figures 19-23: increased blowing produced increased thrust-turning angle, $\theta_R$, with respect to the horizontal, and at constant blowing momentum, increased thrust level resulted in reduced thrust turning caused by the greater kinetic energy in the exhaust which had to be entrained. Also, at a constant power setting, $\%N_1$, increased thrust turning produced a reduced resultant thrust similar to the loss in efficiency experienced with unblown USB configurations (ref. 10). Furthermore, in figures 20-23 there appears to be no hysteresis produced in the thrust turning by increasing (flagged symbols) and then decreasing (unflagged) the thrust over the range of power settings from idle to maximum.

In figure 19 there appears to be an anomaly in the data at lower thrust levels. The turning angle is significantly less than the baseline of Phase I (fig. 24), and the turning angle often decreases at low thrust levels contrary to the rest of the data from both Phase I and Phase II. A possible explanation of this phenomenon is that the CCW trailing edge of this study extended to the approximate edge of the engine jet sheet, and the vortex which is generated at the edge of the jet sheet (ref. 10) lifted the USB jet and separated it from the CCW assembly at low thrusts. This effect would also reduce the turning somewhat at higher thrusts, as can be seen in the case of the CCW with no blowing when it is compared with the plain USB flap. The addition of a fence or end plate inhibits the formation of this edge vortex, and as can be seen in figures 20-23 this flow anomaly no longer exists.

A second difference between the data of Phase I and Phase II is in the amount of turning that occurs on the CCW configurations with no blowing. In figures 20 and 21, the 10-in.-diam, 90° circular arc has approximately the same turning as the USB flap with no CCW device. In figures 22 and 23, the 5-in.-diam, 180° arc turning is slightly higher than the USB flap. This effect of the 5-in.-diam CCW is probably due to its reduced camber compared with the 10-in.-diam Phase I baseline ($r/c = 0.0183$ compared with $r/c = 0.0362$). In the case of the 10-in.-diam, 90° arc, the reason is not so apparent, but it may be related to the combination of a sharp trailing edge with the extension of the Coanda surface through only 90° of arc. In any event, this effect was repeatable and is a decided advantage from a cruise-performance standpoint.

For the smaller 0.035-in. slot heights (figs. 21 and 22), little or no difference was seen in turning between using two or using three start carts to supply the blowing momentum. This is due to the higher plenum pressures required to produce a given momentum with smaller jet-exit areas. Thus, a limiting back pressure was reached (approximately 32-34 psig) above which the start carts could not produce additional mass flow. That is, three carts provide essentially the same momentum as two carts because they are pressure-limited.

In summary, significant thrust deflection was produced by all of the configurations, on the same order or greater, than was produced by the baseline configuration. Individual performance comparisons are made in a following section with a discussion of the differences in the configurations.

Resultant thrust- As mentioned above, the vector resolution of the X-Y static forces acting on the aircraft is termed the resultant thrust, and is assumed to be acting on the aircraft at the thrust deflection angle $\theta_R$, measured positively downward from the aft horizontal. As noted during Phase I (fig. 25) and previous USB investigations, there is usually some loss in resultant thrust as jet turning is increased due to jet spreading, mixing, and viscous losses. For example, in figure 25, at 5000 lb of installed thrust, the thrust recovery varies from 98% without blowing to 89% with the maximum blowing available. For comparison, results for three Phase II configurations are shown. These are the 10-in.-diam, 90° circular arc with both 0.070 in. and 0.035 in. slot heights (figs. 26 and 27), and the 5-in.-diam, 180° circular arc with a 0.035-in. slot height (fig. 28). In general, for similar thrust deflections, resultant thrust recovery is lower with smaller trailing edge radii or larger slot height.

The thrust recovery for the 10-in.-diam, 90° circular arc with a 0.035-in. slot height is about the same as the Phase I baseline, while the 5-in.-diam, 180° circular arc is reduced to 83% at maximum blowing levels.

Thrust resolution- The horizontal and vertical components of resultant thrust are plotted in figure 29 for the baseline configuration at 0.040-in. nominal slot height. Positive $F_X$ is forward thrust, negative $F_X$ is drag. For a constant vertical (lift) force, the addition of blowing reduces the recovered axial force caused by thrust turning. The potential for efficient STOL operation is demonstrated here. For a constant free-stream dynamic pressure, the addition of aerodynamic lift and drag would convert these to lift-drag polars, shifting all the curves upward and to the left (or drag) side of the plot (see refs. 1-3). Operations in flight at a constant vertical (or lift) force could be maintained while horizontal force was being converted from low- to high-thrust recovery by decreasing blowing. This represents conversion from a landing to a wave-off mode. These operations are possible without change in the angle of attack, and require no deflections of moving parts in the high-lift system.

Comparative data for three Phase II configurations are shown in figures 30-32. For similar values of vertical force and momentum, more thrust is recovered with smaller trailing edges of larger slot heights since the turning angles are less. However, more momentum is required to achieve a desired vertical force.

Configuration comparison- A comparison of the thrust-turning performance of the five configurations tested in Phase II and the 0.040-in. slot-height baseline configuration from Phase I is made in figures 33 and 34 for two representative resultant force levels: approximately half-throttle and maximum thrust. Approximately 2° to 4° of additional thrust turning was produced by adding the outboard fence (configuration 2) to the basic 90° circular arc (configuration 1). This simulates a

favorable interference effect, resulting from operation of the outboard engine, that would prevent the inboard exhaust stream from spreading beyond the outboard edge of the blown trailing edge without being entrained. Reduction in slot height (configuration 3) provided an additional thrust deflection of as much as 15° at the same blowing momentum level, depending on the thrust level the engine was producing. This was due to the higher-blowing jet energy at smaller slot heights, which provided greater thrust entrainment. This result was further emphasized when the engine-thrust level was lower (fig. 33) because of the lower exhaust-flow energy that had to be entrained.

Conversion from the 10-in.-diam, 90° circular arc (configurations 2 and 3) to the smaller 5-in.-diam, 180° arc (configurations 4 and 5) produced no thrust-deflection change caused by camber with blowing off, but did produce 8° to 10° less deflection than the larger radius at the higher momentum or thrust levels. This confirms the findings of references 6 and 9, which indicate that flow entrainment over curved surfaces with blowing becomes more difficult with smaller radii, larger slot heights, higher flow velocity and higher blowing-pressure ratios. Also, the data of figures 22 and 23 showed jet deflections exceeded 90° only at very low thrust levels (approximately idle) for the small-radius configuration; the additional 90° of lower surface thus would fulfill little useful purpose at operational thrust levels. The same trailing-edge thickness at the slot location could thus be best used by installing a 90° arc of twice the radius (i.e., configurations 2 and 3).

Of the five new configurations tested, the larger-radius 90° arc with the fence and the reduced slot height (configuration 3) was the most effective over the entire thrust range. In comparison with the Phase I baseline configuration (which had the same radius, a slightly larger slot height, and approximately 170° more of available arc, but a reduced span and no outboard fence), some interesting observations can be made. The effects of reduced span and no end plate appear to be a reduction in thrust turning with blowing $\Delta\theta_R/\Delta\dot{m}V_j$. For the range of blowing tested ($\dot{m}V_j/b_j$ = 0 > 35 lb/ft), the following increases in jet deflection caused by blowing are seen

| Configuration | $T_{resultant}$, lb | $\Delta\theta$, deg |
|---|---|---|
| Baseline, Phase I | 2500 | 26.2 |
| Configuration 3 | 2500 | 46.0 |
| Baseline, Phase I | 5000 | 13.8 |
| Configuration 3 | 5000 | 29.5 |

With the exclusion of the effects of the slightly smaller slot height and the better alignment of the slot lip and trailing edge, the 90° circular arc with smaller slot (configuration 3) roughly doubled the jet deflection caused by the

blowing of the baseline configuration. It thus appears that one of the most effective means to increase jet turning is to ensure that the entire spread exhaust from the USB engine is entrained by the circulation-control jet.

Similar comparisons are seen for the six configurations in figures 35 and 36, where the resulting vertical static forces produced by jet deflection are plotted for two constant horizontal force levels. Again, the 90° circular arc with a smaller slot provides the best lift contribution. It is interesting to note that vertical and horizontal forces are not proportional. Doubling the horizontal force 2500 to 5000 lb produces less than a doubling in resultant vertical force at the same blowing momentum because of the increased difficulty in deflecting the higher-energy jet velocities.

An important advantage relative to blowing-off cruise flight of a CCW/USB configuration can also be noted in figures 33 and 34. The unblown geometric camber of the large-radius, circular, trailing-edge baseline configuration produces significant thrust deflection by itself: between 27° and 31° for the thrust levels shown. This is 8° to 11° greater than the undeflected sharp trailing-edge flap of the basic QSRA, and represents a reduced horizontal force component during cruise in addition to a reduced resultant thrust caused by scrubbing and mixing losses. On the other hand, the 90° circular arc produces unblown thrust deflections only 1° to 2° greater than the basic undeflected flap of the QSRA; thus there is little loss in effective horizontal thrust for the aircraft caused by the presence of the CCW.

Jet-blowing momentum- A goal of the present tests was to investigate additional thrust deflection possible with greater available mass flow to power the system. That goal was not accomplished because of the pressure limitations of the ground air-start carts. However, the effect of additional mass flow and momentum is implied by figures 33-36; greater thrust deflection and vertical force generation continue to result with no limitation noted from the present data. However, indications from references 6 and 9 are that the smaller radii, larger slot-height configurations will eventually reach a jet-pressure ratio where flow turning will begin to decrease as a result of additional blowing. That limit will not be determined until higher-pressure air-supply systems are available.

Since a STOL aircraft employing the CCW/USB concept would most likely supply the blowing momentum from engine bleed air, figure 37 provides useful design information in terms of momentum required as a fraction of installed engine thrust. The 90° circular arc configuration can produce 60° of thrust deflection for a midrange power setting using bleed momentum that is only 5% of the thrust. Since turbine-engine thrust loss can become appreciable with bleed (see ref. 11, for example), it is desirable to keep this bleed value as low as possible for takeoff and climb-out. From this standpoint, it is interesting to note that a typical thrust deflection of 45° can be produced by the 90° circular arc configuration using bleed equal to 1.8% of the installed thrust, compared to 3.2% for the 5-in.-diam circular arc, or 3.7% for the baseline configuration. This represents a significant decrease in required bleed momentum for the best configuration.

## CONCLUDING REMARKS

The ability of the CCW/USB concept to deflect engine thrust to angles greater than 90° was verified in a full-scale ground test conducted on the QSRA in 1981. This investigation, referred to as Phase I, was undertaken to confirm that full-scale static-thrust deflection could be accomplished by the CCW/USB concept; to compare that thrust turning to model-scale results; and to identify any problems associated with the full-scale airplane and engine. During this Phase I investigation, the full-scale CCW/USB system demonstrated thrust turning ranging from 97° to 40°, depending on the thrust level. However, the blowing momentum required for thrust angle change was higher than expected, based on model-scale data. In addition, analysis and observation indicated smaller slot heights were required, and only part of the jet sheet was being turned.

A second study, Phase II, was accomplished in August 1983 with an improved CCW design to continue the testing of Phase I, to investigate and alleviate the problems identified in Phase I, and to investigate improved CCW/USB geometry which would be more representative of flight hardware. Five new configurations were tested over a range of engine thrust and CCW blowing momentum. Comparisons of their performance improvements and thrust-deflecting capabilities have led to the following comments and conclusions:

1. Compared to the Phase I baseline configuration, CCW blowing-momentum values up to 35 lb/ft of blowing slot produced the same or greater thrust deflection angles, ranging from 40° to 102°, depending on thrust level. As before, increased thrust levels produced reduced thrust turning caused by higher jet-energy levels, and at a constant power setting, increased thrust turning caused by blowing yielded reduced resultant thrust because of scrubbing and mixing losses.

2. Maximizing flow entrainment by using an end plate (fence) to simulate the presence of flow from an adjacent engine adds 2° to 4° additional thrust turning to a given configuration at high thrust levels. However, the addition of the end plate stabilized the turning flow, particularly at the lower thrust and blowing levels. It is highly likely that one or more fences or end plates would be required in a practical configuration to stabilized engine-out CCW operation.

3. Reducing the slot height by 50% adds 8° to 15° thrust deflection to a given configuration at the same blowing momentum; the exact amount of increase is dependent on engine thrust level. In addition to the thrust-deflection improvement, the flow-turning efficiency is also improved, and lies within the performance band for normal USB flaps. The 10-in.-diam, 90° arc has a turning efficiency between 98% and 89%, depending on thrust and turning angle, which is in the same range as a very good USB flap.

4. Reducing the trailing-edge radius by 50% (comparing the 5-in.-diam, 180° arc relative to the 10-in.-diam, 90° arc) reduces thrust turning by 8° to 10°.

5. The most effective trailing-edge configuration from a thrust-turning standpoint was found to be the 90° circular arc. It provided the same thrust turning as the other configurations while using considerably less momentum, or produced greater thrust turning at the same momentum. Exact comparison with the baseline circular cylinder of Phase I is not possible because of span and other geometry differences, but indications are that any additional physical arc greater than 90° performs little useful function.

6. The 90° circular arc produces essentially no thrust deflection because of camber without blowing. This indicated that a high-performance CCW/USB can be designed with little if any horizontal thrust loss during cruise. In addition, although not evaluated, the cruise drag of the thinner 90° circular arc should be less than the baseline full cylinder, and less than the smaller-radius 180° circular arc because of its bluffness and tendency toward flow separation.

7. Although it was not possible to investigate higher mass flow and momentum because of limitations on the air supply, the data imply that additional gains can be made with higher-pressure air systems.

These results confirm improvements in the CCW/USB concept which increase its feasibility as a versatile and effective STOL concept. The 90° circular arc has demonstrated that adequate pneumatic thrust turning can be produced by a trailing-edge shape which may have minimal cruise-performance penalty. That is, little thrust loss is caused by camber-induced thrust deflection and the base drag should be reasonable. Reduced slot height, increased blowing system span, and the favorable outboard-engine interface confirm that significant thrust deflection can be achieved at considerably lower blowing momentum than was required with the baseline configuration in Phase I. The CCW/USB ability to control horizontal forces and produce either thrust or drag while maintaining a constant vertical force thus continues to be obtainable from a simple, thinner trailing edge, which appears to be more satisfactory from a cruise drag standpoint. In addition, the CCW/USB concept would eliminate the large flap brackets and fairings which are responsible for a significant amount of weight and drag, resulting in a cleaner wing. Finally, the CCW/USB flap concept could lead to a reduced-chord (for the same thickness) wing which could reduce engine-exhaust scrubbing drag and improve wing-aspect ratio, offsetting any additional drag caused by the CCW trailing edge.

The viability of this CCW/USB system for STOL operations is due to its versatility in controlling horizontal forces to produce either thrust or drag while maintaining a constant, large vertical force. These forces are controlled by changing the amount of blowing, either inboard or outboard, or both, thus allowing rapid readjustment of the spanwise circulation and of the load distribution on the wing. Depending on mission requirements, this system could have significant advantages over a mechanical-flap design. For example, an advanced CCW/USB pneumatic control system could be used on a high-speed fighter to provide substantially increased maneuverability without conventional control-surface speed boundaries; and the system's use on a super-STOL would make it possible to trade maximized acceleration during the initial takeoff run for high lift at rotation. The transition from

landing to wave-off configurations could be achieved rapidly by changing the blowing pressure in the ducts, a procedure that does not require any moving external parts.

The ultimate test of this CCW/USB thrust-deflecting system would be accomplished through large-scale wind tunnel tests and finally, a flight demonstration on the QSRA aircraft. It is recommended that such an undertaking be considered.

Ames Research Center
National Aeronautics and Space Administration
Moffett Field, California
August 29, 1986

## REFERENCES


1. Nichols, J. H., Jr.; and Englar, R. J.: Advanced Circulation Control Wing System for Navy STOL Aircraft. AIAA Paper 80-1825, Anaheim, Calif., Aug. 1980.

2. Nichols, J. H., Jr.; Englar, R. J.; Harris, M. J.; and Huson, G. G.: Experimental Development of an Advanced Circulation Control Wing System for Navy STOL Aircraft. AIAA Paper 81-0151, St. Louis, Mo., Jan. 1981.

3. Harris, M. J.: Investigation of the Circulation Control Wing/Upper Surface Blowing High-Lift System on a Low Aspect Ratio Semispan Model. Report ASED-81/10, David Taylor Naval Ship Research and Development Center, Bethesda, Md., May 1981.

4. Englar, Robert J.; Furey, Roger J.; Lee, David J.; and Nichols, James H., Jr.: Thrust Deflector and Force Augmenter. U.S. Patent No. 4,398,687, 16 August 1983, and U.S. Patent No. 4,463,920, 7 August 1984.

5. Eppel, J. C.; Shovlin, M. D.; Jaynes, D. N.; Englar, R. J.; and Nichols, J. H., Jr.: Static Investigation of the Circulation Control Wing/Upper Surface Blowing Concept Applied to the Quiet Short-Haul Research Aircraft. NASA TM-84232, 1982.

6. Englar, R. J.: Experimental Investigation of the High Velocity Coanda Wall Jet Applied to Bluff Trailing Edge Circulation-Control Airfoils. Report 4708, Naval Ship Research and Development Center, Bethesda, Md., Sept. 1975. Report No. AD-A019417 AERO-1213 TN-AL-308.

7. Shovlin, M. D.; Skavdahl, H.; and Harkonen, D. L.: Design and Performance of the Propulsion System for the Quiet Short-Haul Research Aircraft (QSRA). AIAA Paper 79-1313, June 1979.

8. Eppel, J. C.: Quiet Short-Haul Research Aircraft Familiarization Document, Revision 1. NASA TM-81298, Sept. 1981.

9. Englar, R. J.: Low-Speed Aerodynamic Characteristics of a Small, Fixed-Trailing-Edge Circulation Control Wing Configuration Fitted to a Supercritical Airfoil. Report AESD-81/08, Naval Ship Research and Development Center, Bethesda, Md., March 1981.

10. Phelps, A. E., III; Johnson, J. L., Jr.; and Margason, R. J.: Summary of Low-Speed Aerodynamic Characteristics of Upper-Surface Blown Jet-Flap Configurations. In NASA SP-406, May 24-26, 1976, pp. 63-87.

11. Englar, R. J.; Hemmerly, R. A.; Moore, W. H.; Seredinsky, V.; Valckenaere, W.; and Jackon, J. A.: Design of the Circulation Control Wing STOL Demonstrator Aircraft. AIAA Paper 79-1842, New York, N.Y., Aug. 1979.

TABLE 1.- TEST PROGRAM SUMMARY--QSRA CCW/USB PHASE II, 25-31 AUGUST 1983
ENGINE NO. 2 (LEFT INBOARD)

| Revised run numbers | Config-uration number | Trailing edge configuration | Pressurized slot height, in. | Fence | Engine power setting | Air start carts | Comments | |
|---|---|---|---|---|---|---|---|---|
| 2-16 | 1 | 10-in.-diam 90° circ arc | 0.070 | OFF | Idle → Max | 0 | Thrust deflection, h = 0.070 in. | |
| 58-72* | | | | | | | | |
| 93-107 | | | | | | 1 (M) | | |
| 17-40* | | | | | | | | |
| 79-92 | | | | | | 2 (O+I) | | |
| 44-57* | | | | | | 3 | | |
| 73*, 108 | | | | | OFF | 1 | Jet turning, | CCW alone |
| 75*, 109 | | | | | | 2 | | |
| 74* | | | | | | 3 | | |
| 112-126 | 2 | | | ON | Idle → Max | 0 | Effect of fence | |
| 127-141 | | | | | | 2 | | |
| 142-156 | | | | | | 3 | | |
| 157-171 | | | | | | 1 | | |
| 172 | | | | | OFF | 1 | | CCW alone |
| 174 | | | | | | 2 | | |
| 173 | | | | | | 3 | | |
| 177-191 | 3 | | .035 | | Idle → Max | 2 | Reduced slot ht | |
| 192-206 | | | | | | 3 | | |
| 207-221 | | | | | | 1 | | |
| 222 | | | | | OFF | 1 | | CCW alone |
| 223 | | | | | | 3 | | |
| 224 | | | | | | 2 | | |
| 227-241 | 4 | 5-in.-diam 180° circ arc | | | Idle → Max | 0 | Smaller T.E. | |
| 242-256 | | | | | | 2 (M+I) | | |
| 257-266 | | | | | | 2 (O+I) | | |
| 267-281 | | | | | | 3 | | |
| 282-296 | | | | | | 1 (M) | | |
| 297-311 | 5 | | .070 | | | 2 (O+I) | Increased slot ht | |
| 312-326 | | | | | | 3 | | |
| 327-341 | | | | | OFF | 1 | | |
| 342 | | | | | | 1 | | CCW alone |

TABLE 1.- CONCLUDED

| Revised run numbers | Config-uration number | Trailing edge configuration | Pressurized slot height, in. | Fence | Engine power setting | Air start carts | Comments |
|---|---|---|---|---|---|---|---|
| 343 | 5 | 5-in.-diam 180° circ arc | 0.070 | ON | OFF | 3 | Increased slot ht, CWW alone |
| 344 | 5 | 5-in.-diam 180° circ arc | 0.070 | ON | OFF | 2 (O+I) | Increased slot ht, CWW alone |
| 347-360 | Basic QSRA | Conv. USB, $\delta_{USB}$ = 0° | --- | OFF | Idle → Max | 0 | Engine #3, #4 Off |
| 362-374 | ↓ | ↓ | ↓ | ↓ | ↓ | ↓ | Engine #3, #4 Idle |
| 375-387 | | | | | | | Engine #4, #3 Idle |
| 388-400 | | | | | | | Engine #3 + #4 |
| 401-415 | | | | | | | Engine #4, #3 Off |

Notes: 1. Carts: O = Outbd, M = Middle, I = Inbd
2. * = Instrumentation problem - data may be questionable.
3. Engines: 1 = Left Outbd, 2 = L. Inbd, 3 = Right Inbd, 4 = R. Outbd.

TABLE 2.- SUMMARY OF PHASE II CONFIGURATIONS

| Configuration | Trailing edge | Slot height, in. | Fence | Span, in. |
|---|---|---|---|---|
| 1 | 10-in.-diam, 90° circular arc | 0.070 | Off | 88.0 |
| 2 | 10-in.-diam, 90° circular arc | .070 | On | |
| 3 | 10-in.-diam, 90° circular arc | .035 | | |
| 4 | 5-in.-diam, 180° circular arc | .035 | | |
| 5 | 5-in.-diam, 180° circular arc | .070 | | |
| Phase I, Baseline | 10-in.-diam, 260° circular arc | 0.040-0.067 | Off | 75.0 |

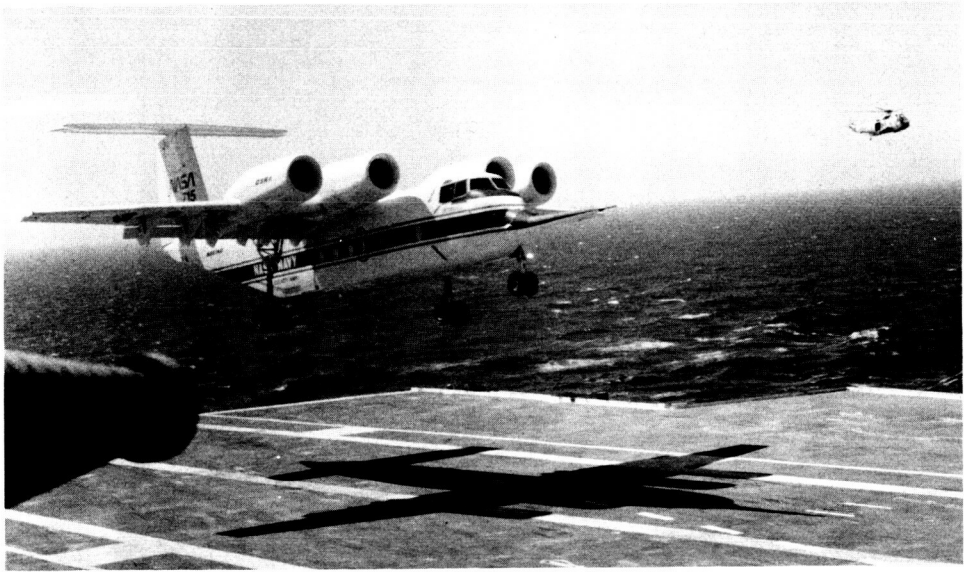

Figure 1.- Quiet Short-Haul Research Aircraft.


Figure 2.- A-6/CCW Flight Demonstrator Aircraft.

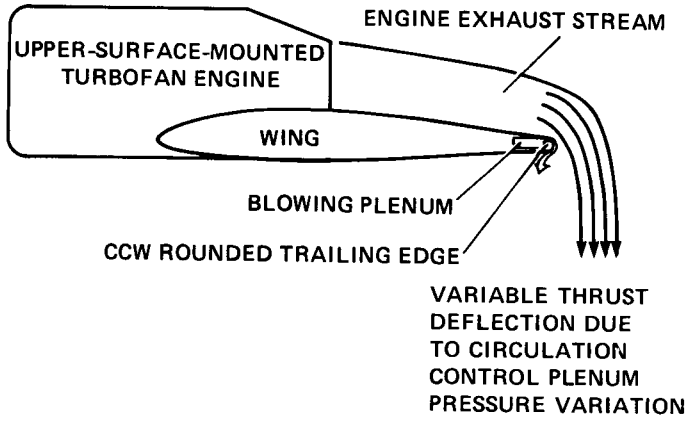


Figure 3.- CCW/USB thrust deflector and lift augmentation concept.

AERODYNAMIC DATA

| | WING | HORIZ | VERT |
|---|---|---|---|
| AREA (TRAP), $ft^2$ | 600.0 | 233.0 | 152.0 |
| SPAN, ft | 73.5 | 32.0 | 14.0 |
| ASPECT RATIO | 9.0 | 4.4 | 1.22 |
| TAPER RATIO | 0.30 | 0.75 | 0.60 |
| SWEEP, C4, deg | 15.0 | 3.0 | 18.0 |
| M.A.C. in. | 107.4 | 88.0 | 137.0 |
| CHORD ROOT, in. | 150.7 | 100.0 | 168.0 |
| CHORD TIP, in. | 45.2 | 75.0 | 100.0 |
| T/C BODY SIDE, % | 18.54 | 14 | 14 |
| T/C TIP, % | 15.12 | 12 | 14 |
| INCIDENCE, deg | 4.5 | – | – |
| DIHEDRAL, deg | 0.0 | – | – |
| TAIL ARM, in. | – | 525.0 in. | 488.0 in. |
| VOL COEFF V | – | 1.898 | 0.1402 |

CONTROL SURFACES

| $ft^2$/APL * | | BLOWN |
|---|---|---|
| AILERON | 32.2 | BLC |
| FLAPS INBD | 105.0 | USB |
| FLAPS OUTBD | 40.2 | NONE |
| SPOILERS | 33.7 | NONE |
| L.E. FLAPS | 54.3 | NONE |
| ELEVATOR | 81.6 | NONE |
| RUDDER | 60.8 | NONE |

*THEORETICAL RETRACTED AREA

PROPULSION

| | |
|---|---|
| ENGINE | LYCOMING YF-102 |
| STATIC THRUST | 6225** |
| FAN P.R. | 1.45 |
| BY-PASS RATIO | 6.0 |

**MEASURED THRUST

LANDING GEAR

| GEAR | STROKE | TIRE | TIRE O.D. | ROLLING R. |
|---|---|---|---|---|
| MLG, in. | 21.0 | 14x15 | 37 | ~ 15.2 |
| NLG, in. | 17.5 | 8.90-12.50 TYPE III | 27.5 | 12.0 |

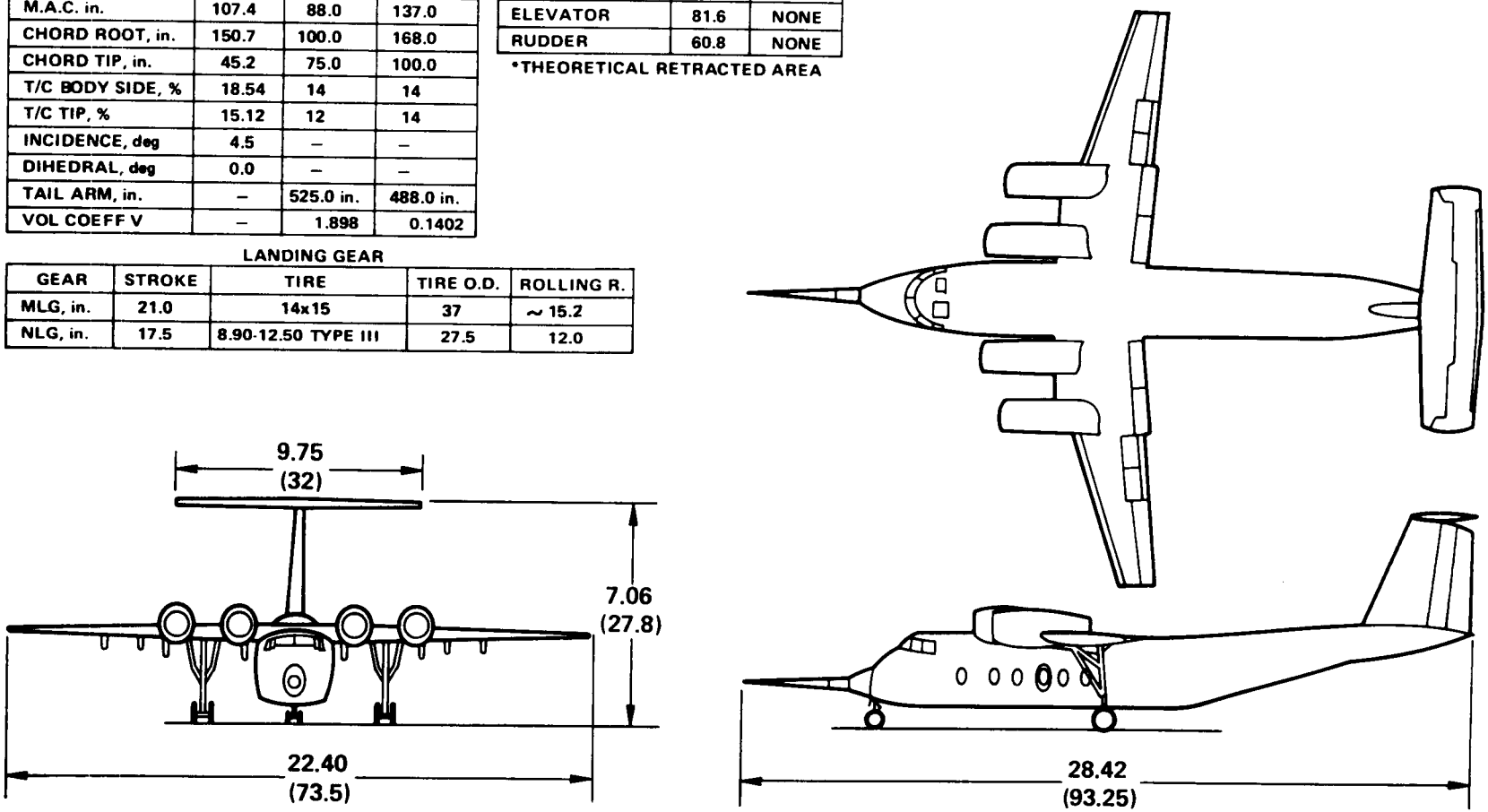


DIMENSIONS IN m(ft)

Figure 4.- QSRA design and configuration data.

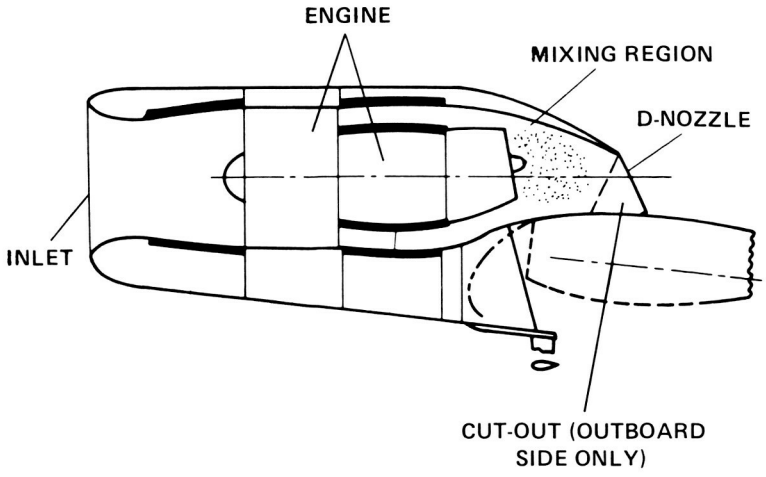


Figure 5.- QSRA nacelle.

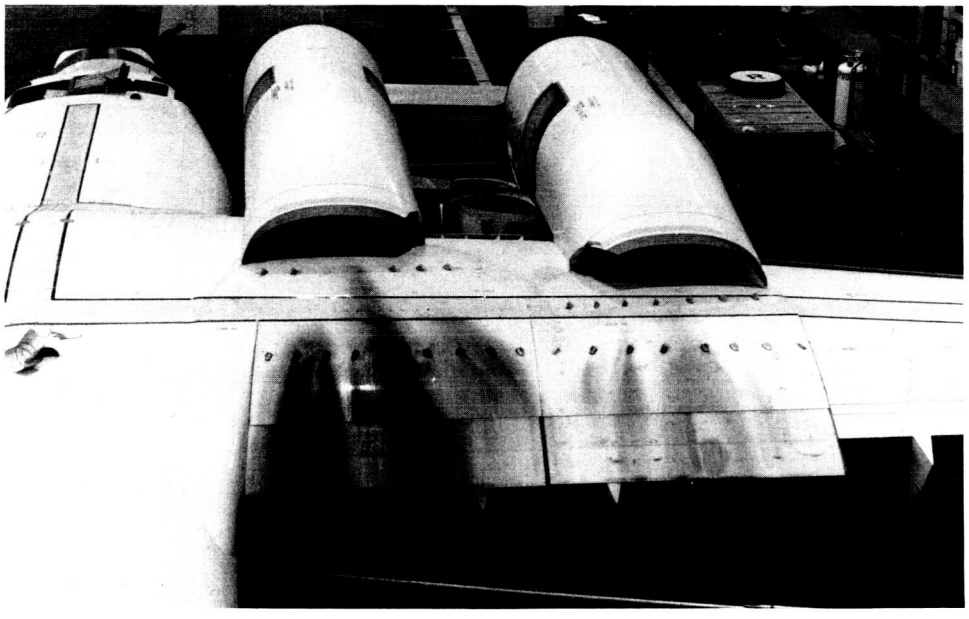

Figure 6.- Top view of QSRA showing engine nozzle cutouts and vortex generators.

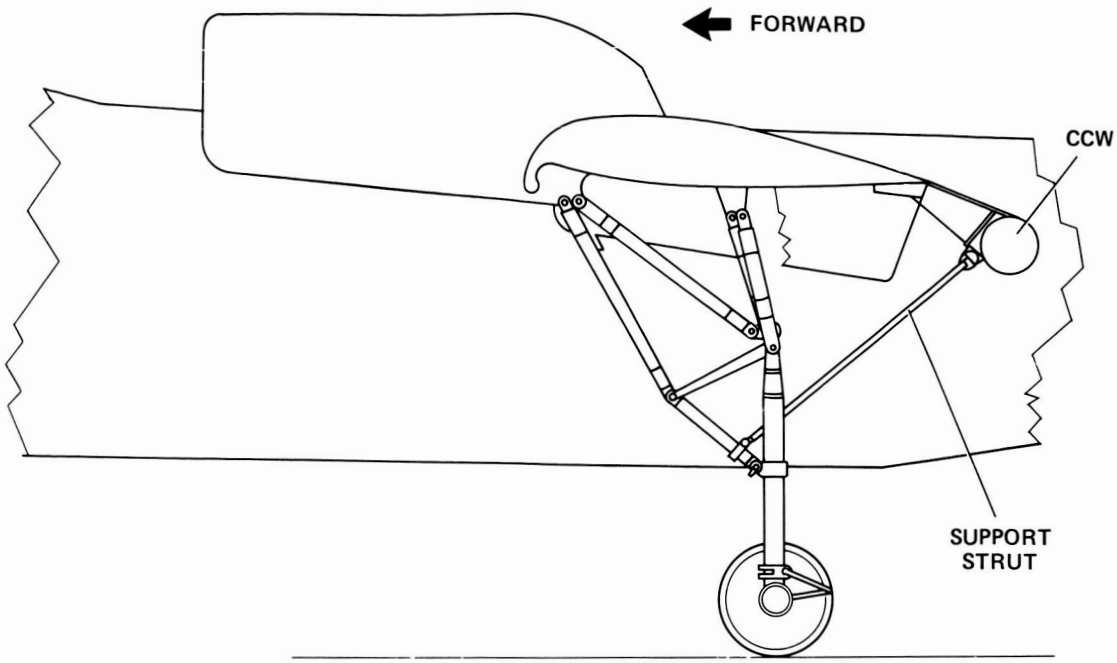


Figure 7.- CCW flap installed on the QSRA.

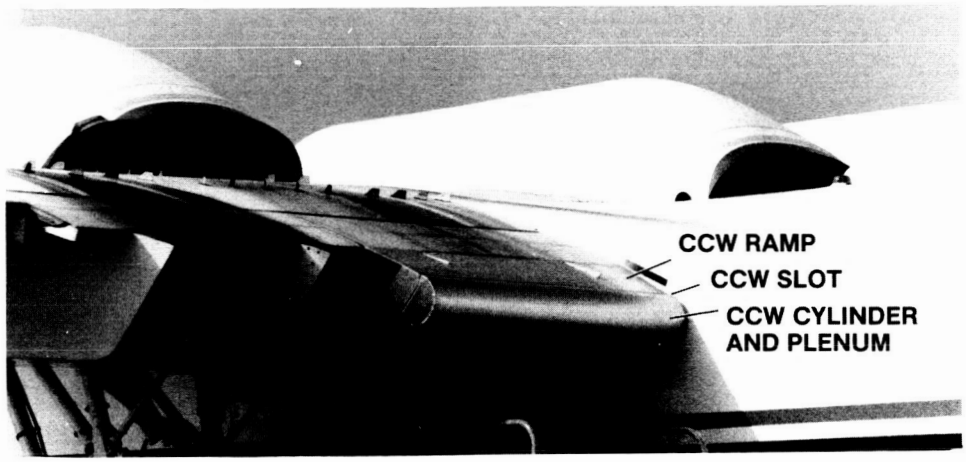


Figure 8.- CCW/USB assembly installation during Phase I.

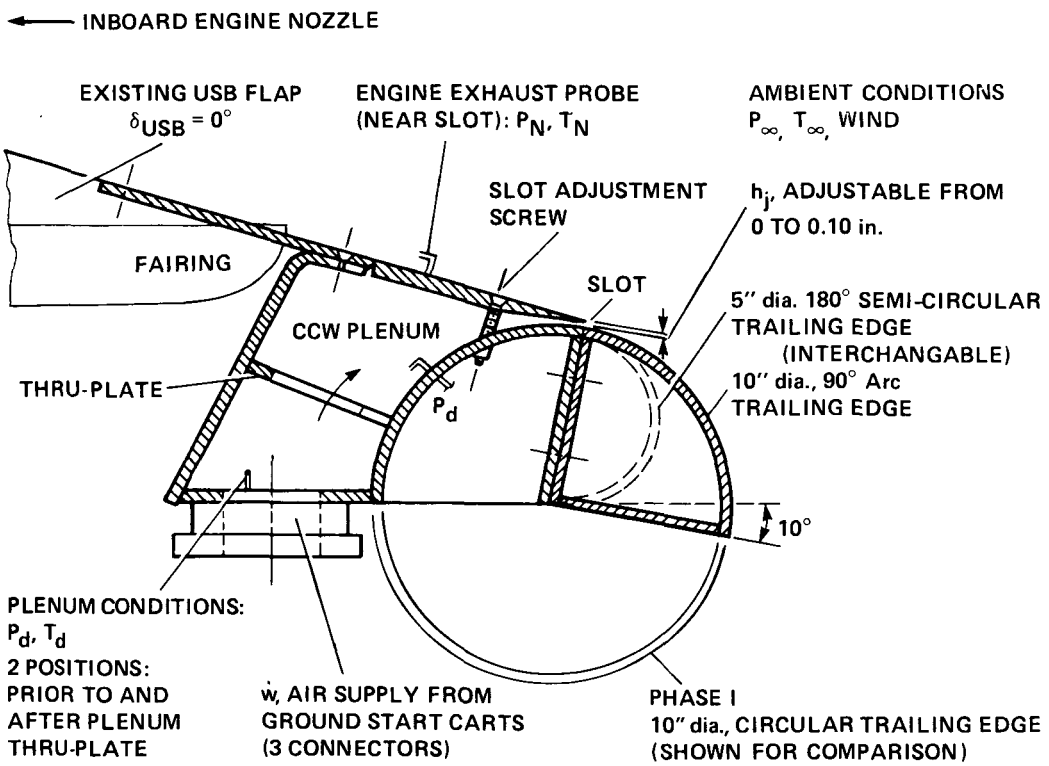


Figure 9.- CCW/USB Phase II trailing edge assembly, installation, and test parameters.

Figure 10.- End view of the 10-in.-diam, 90° arc CCW flap installed on the QSRA.

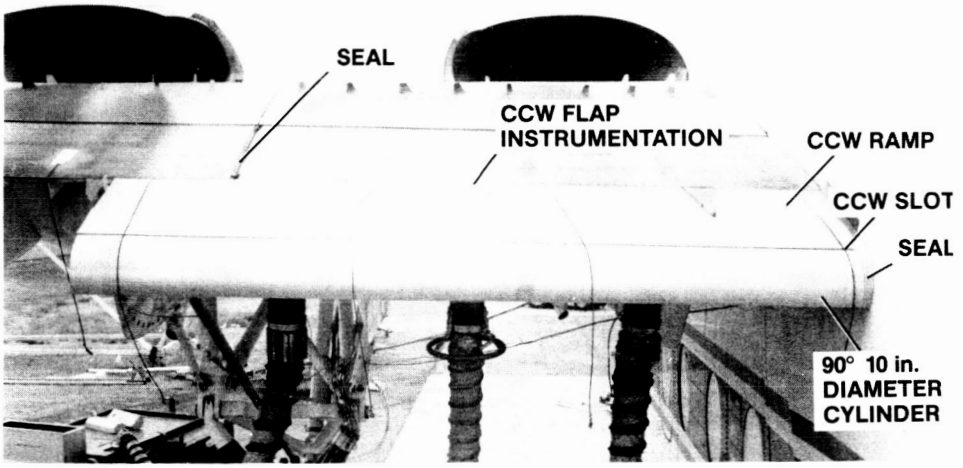


Figure 11.- The 10-in.-diam, 90° arc CCW flap installed on the QSRA.

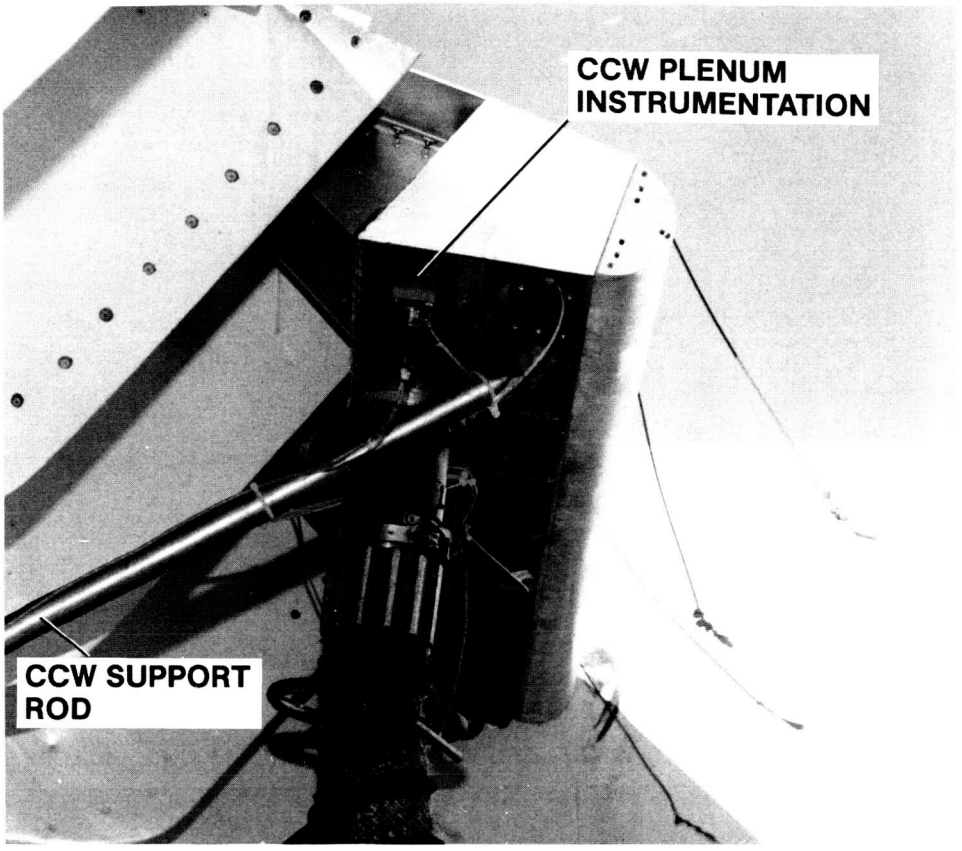


Figure 12.- End view of the 5-in.-diam, 180° arc CCW flap installed on the QSRA.

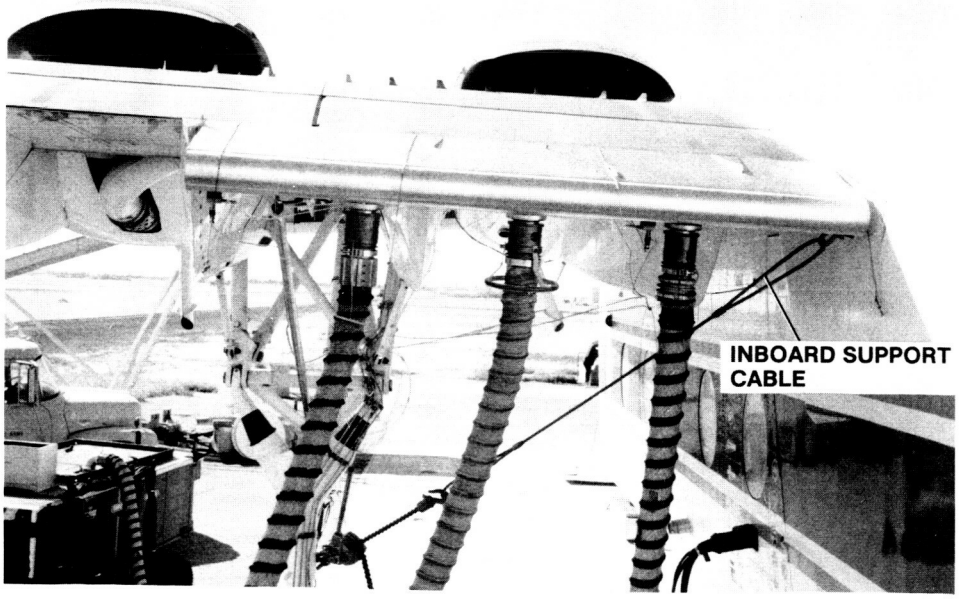


Figure 13.- The 5-in.-diam, 180° arc CCW flap installed on the QSRA.

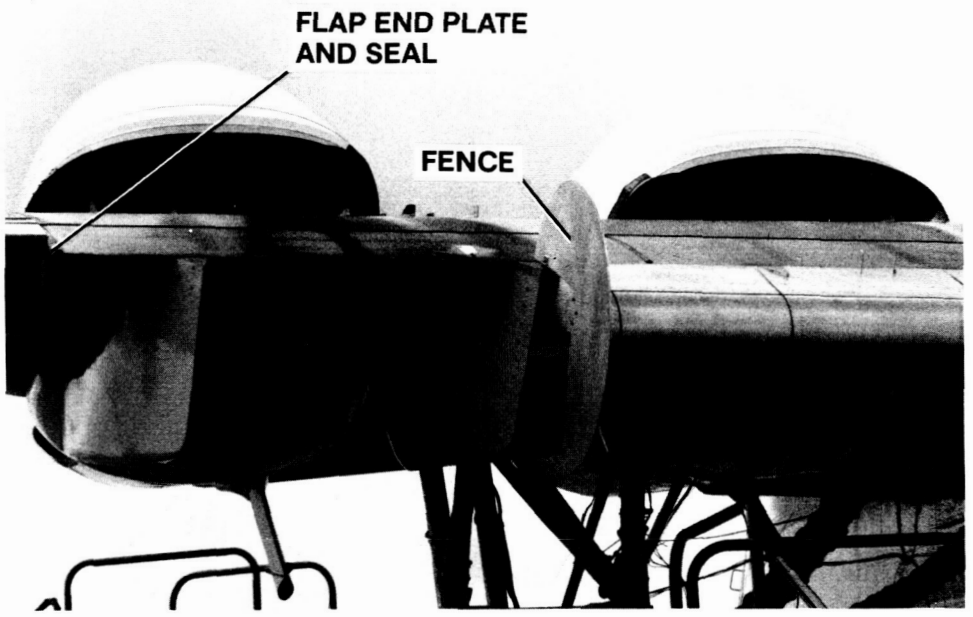


Figure 14.- The 10-in.-diam, 90° arc CCW flap with end plate (fence) installed on the QSRA.


Figure 15.- The QSRA main- and nose-gear load-pad installations.

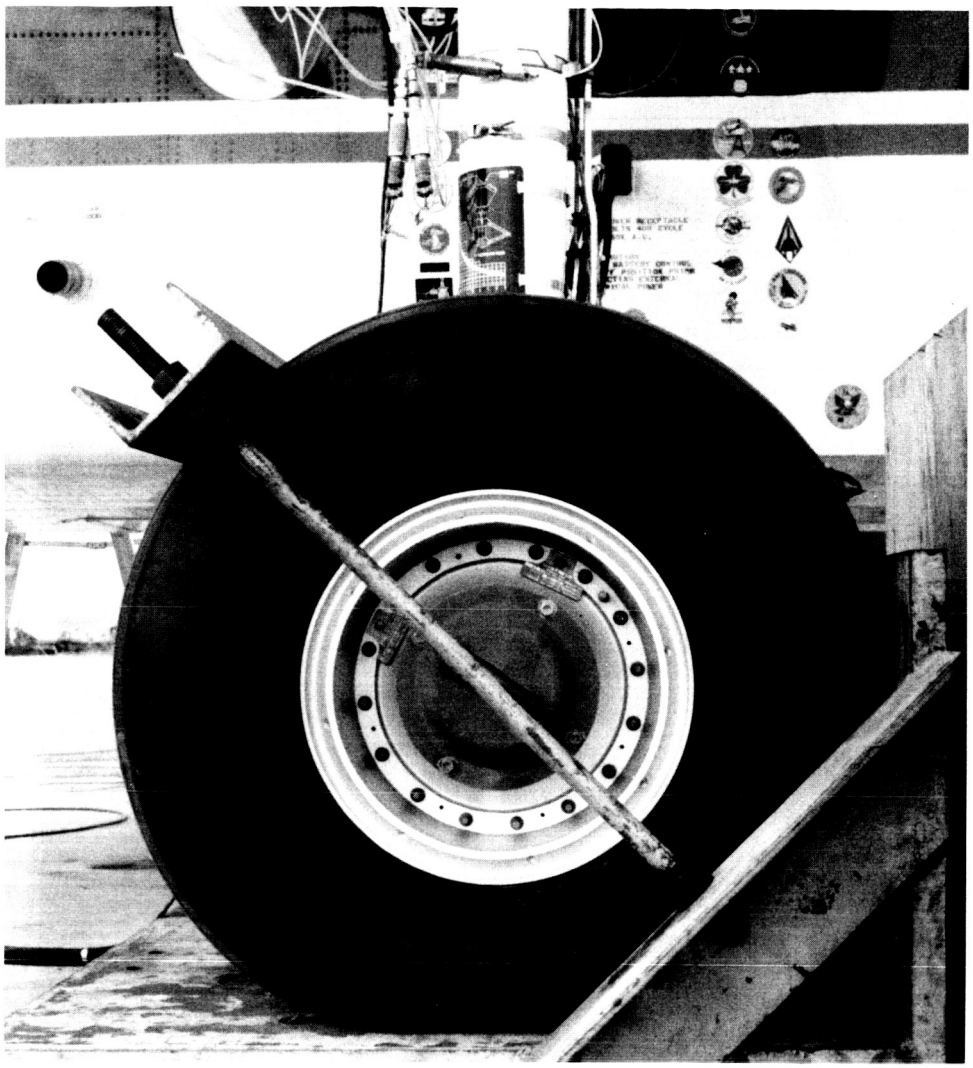

Figure 15.- Concluded.

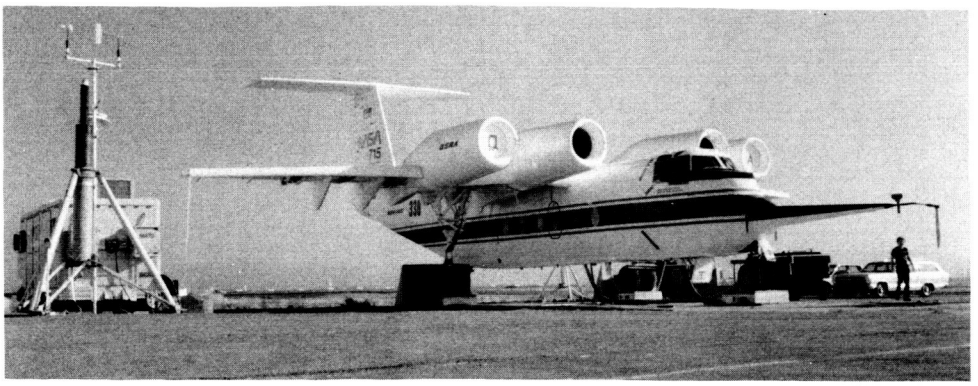

Figure 16.- Overall view of the QSRA installed on the load pads and the weather station.

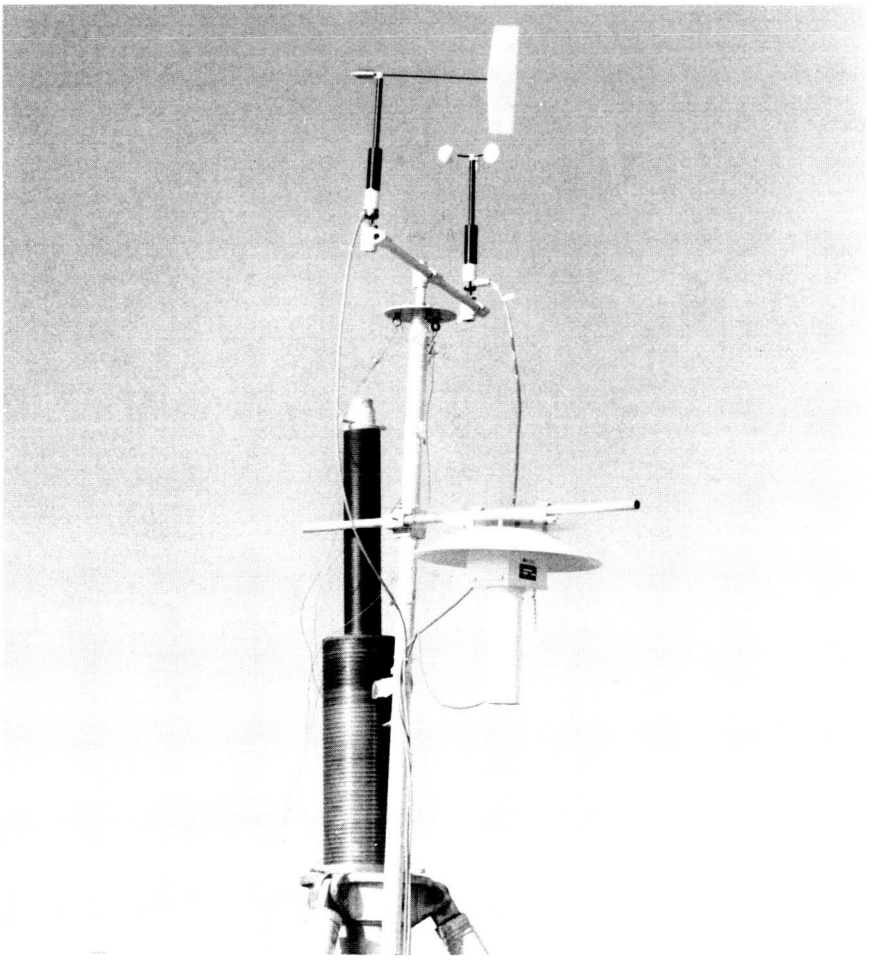

Figure 17.- View of the weather station showing the wind direction, speed and temperature sensors.

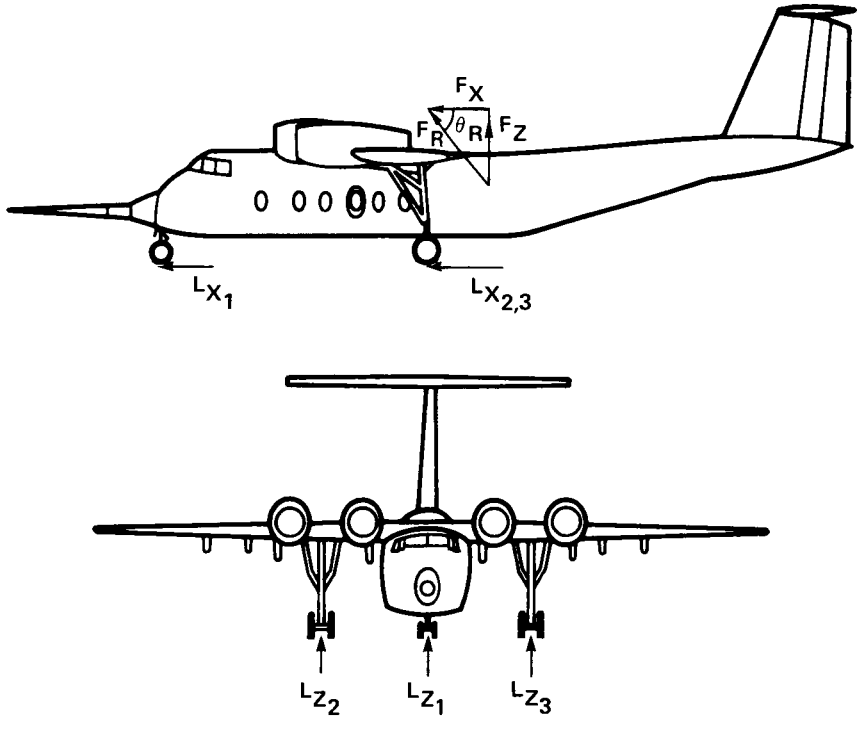


Figure 18.- Location and direction of the forces acting on the aircraft.

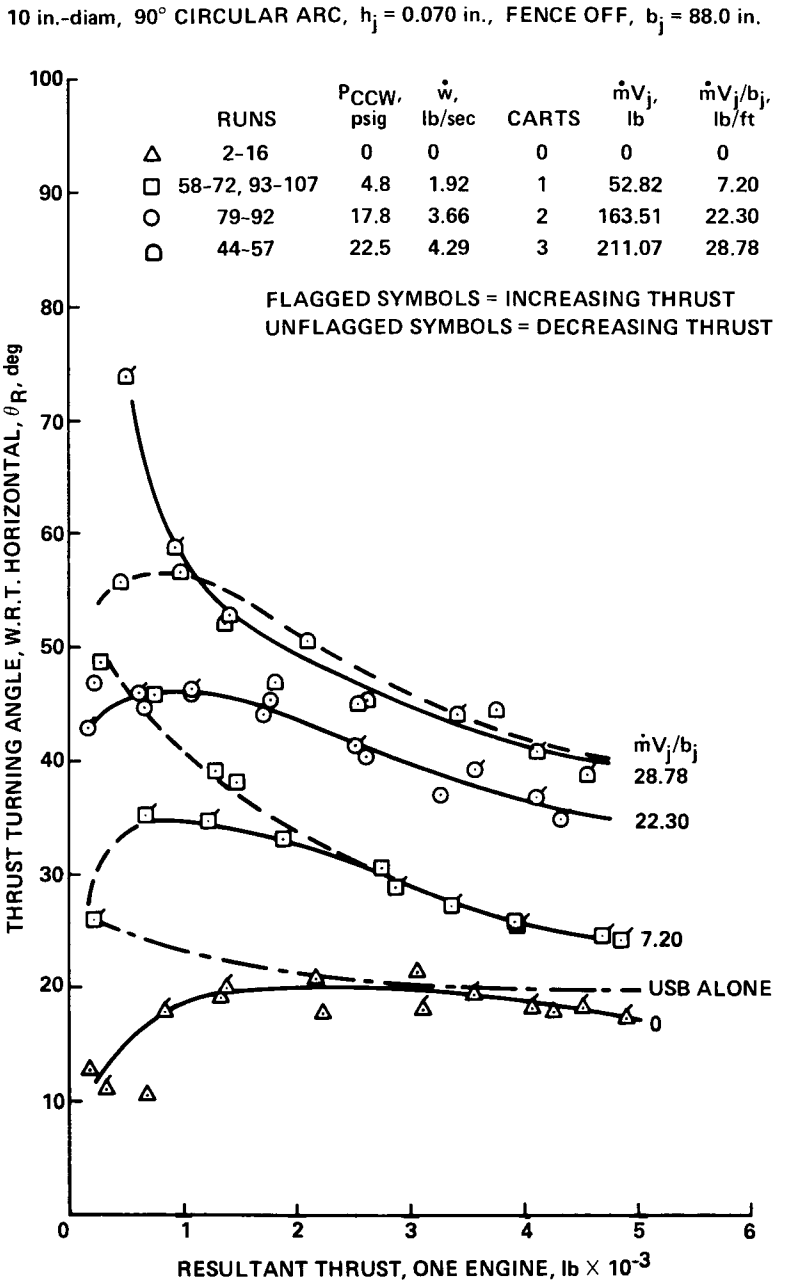


Figure 19.- Static thrust turning angle, configuration 1.

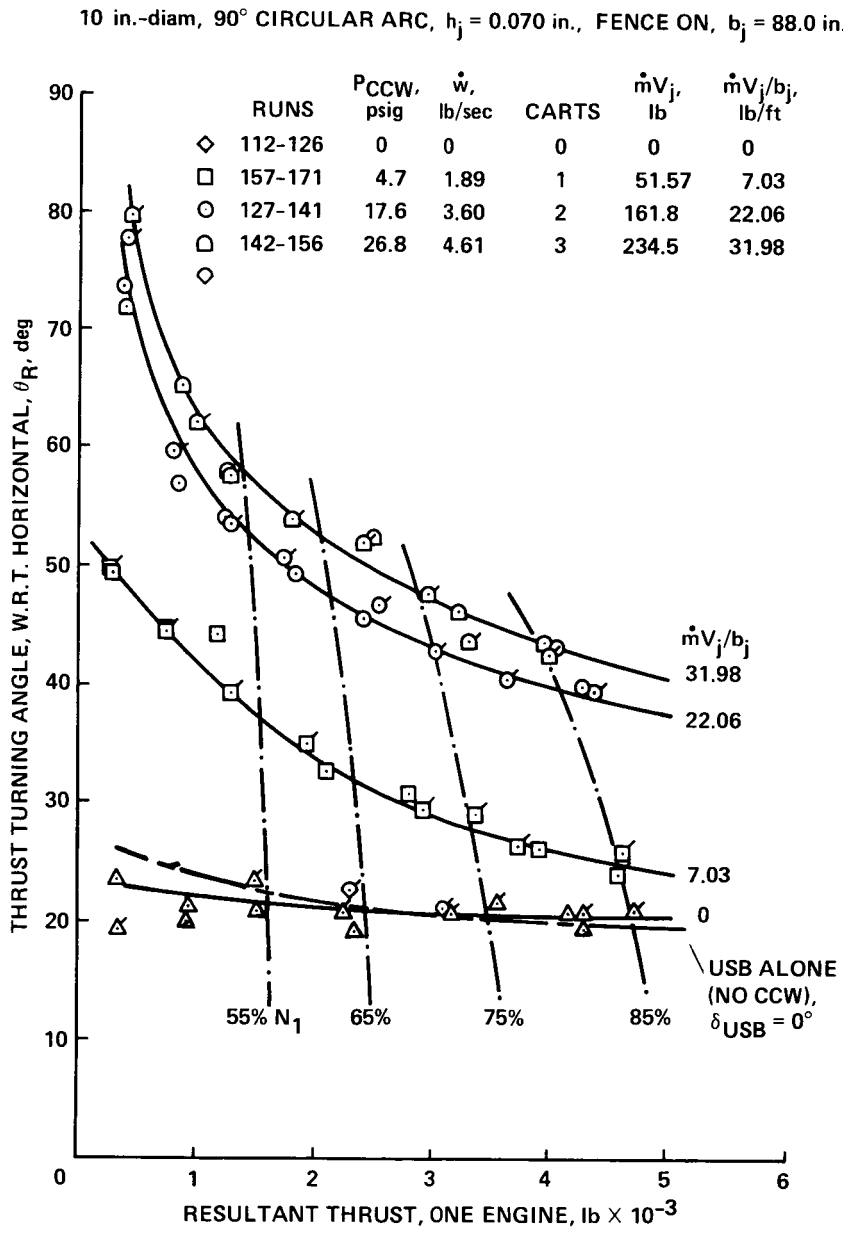


Figure 20.- Static thrust turning angle, configuration 2.

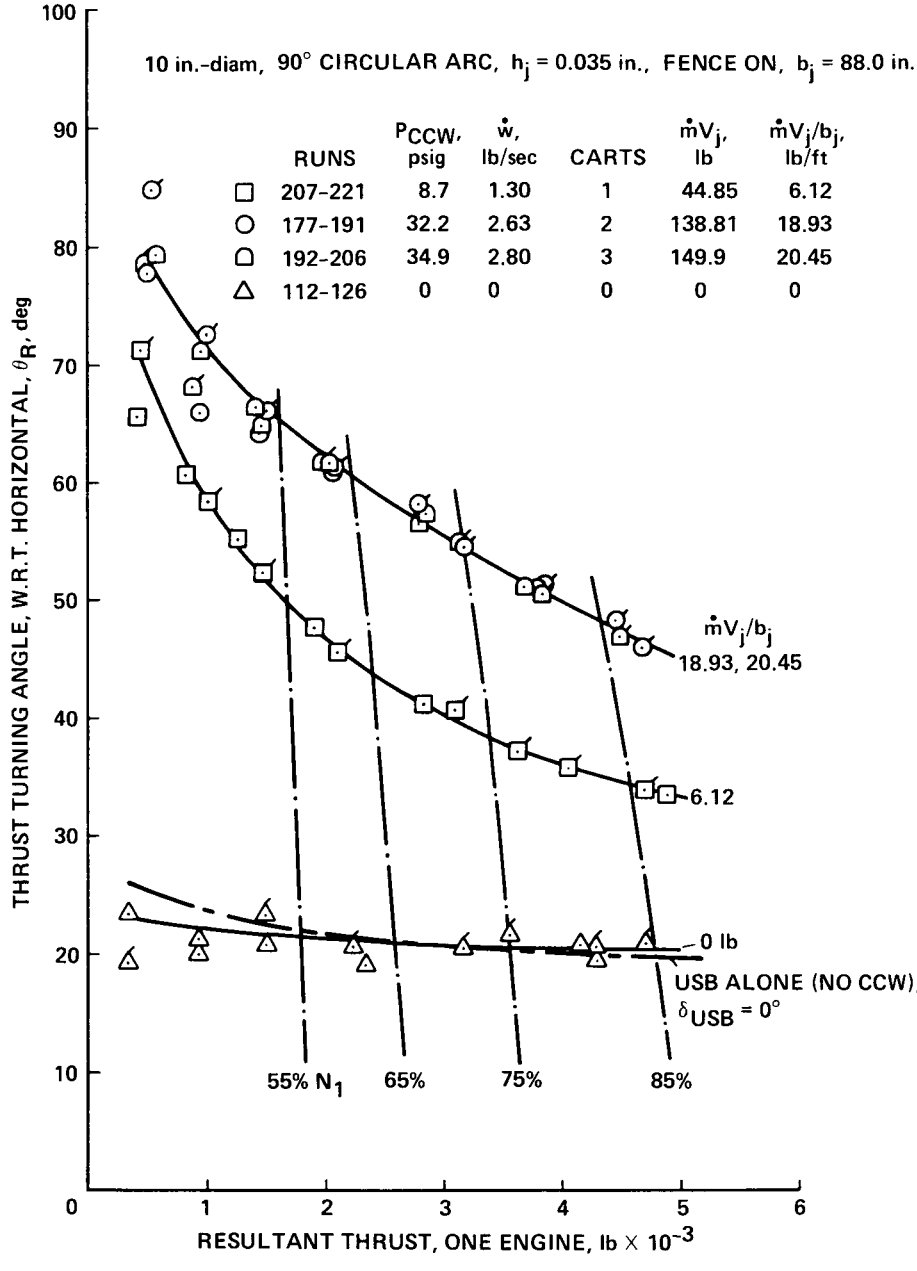


Figure 21.- Static thrust turning angle, configuration 3.

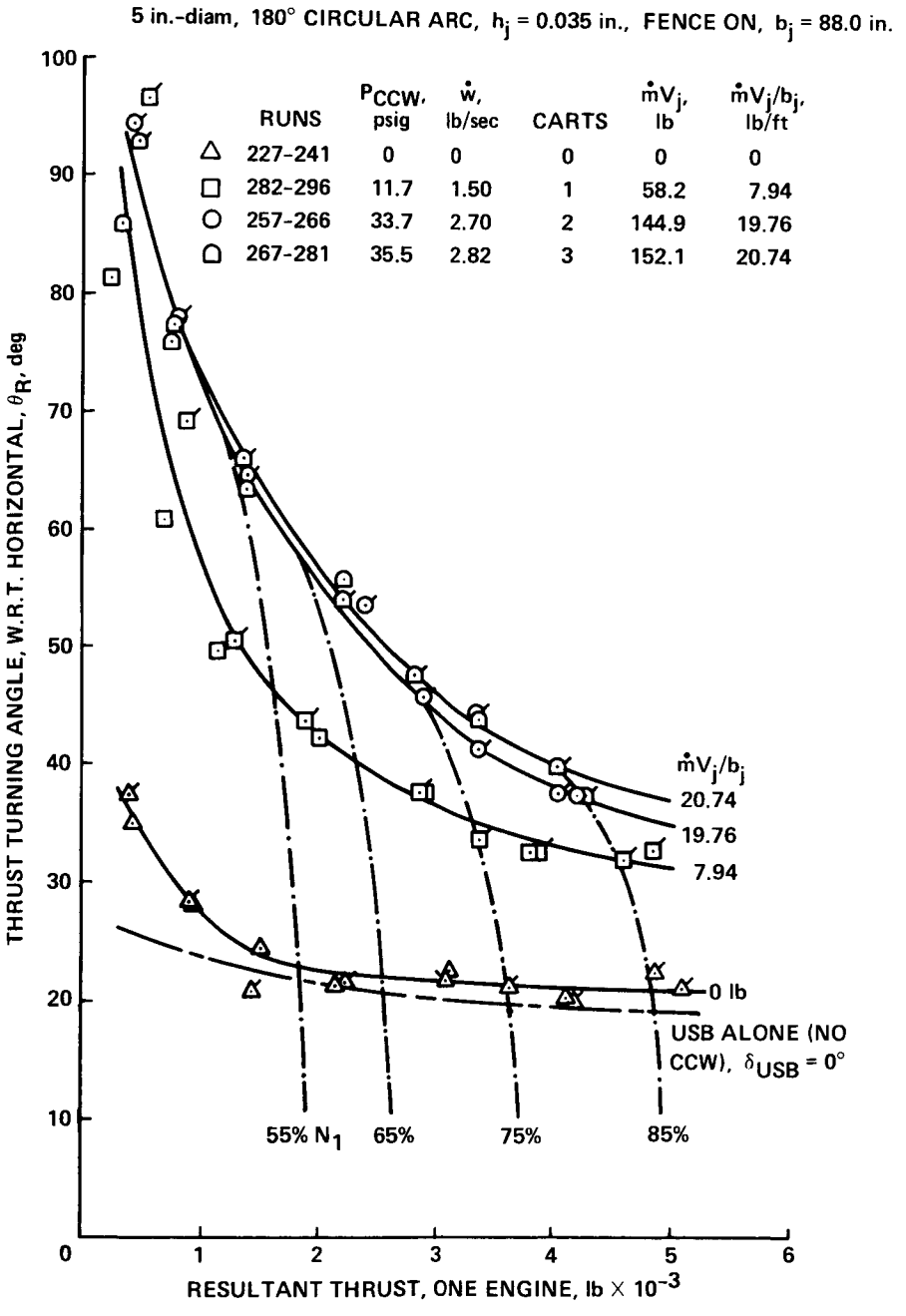


Figure 22.- Static thrust turning angle, configuration 4.

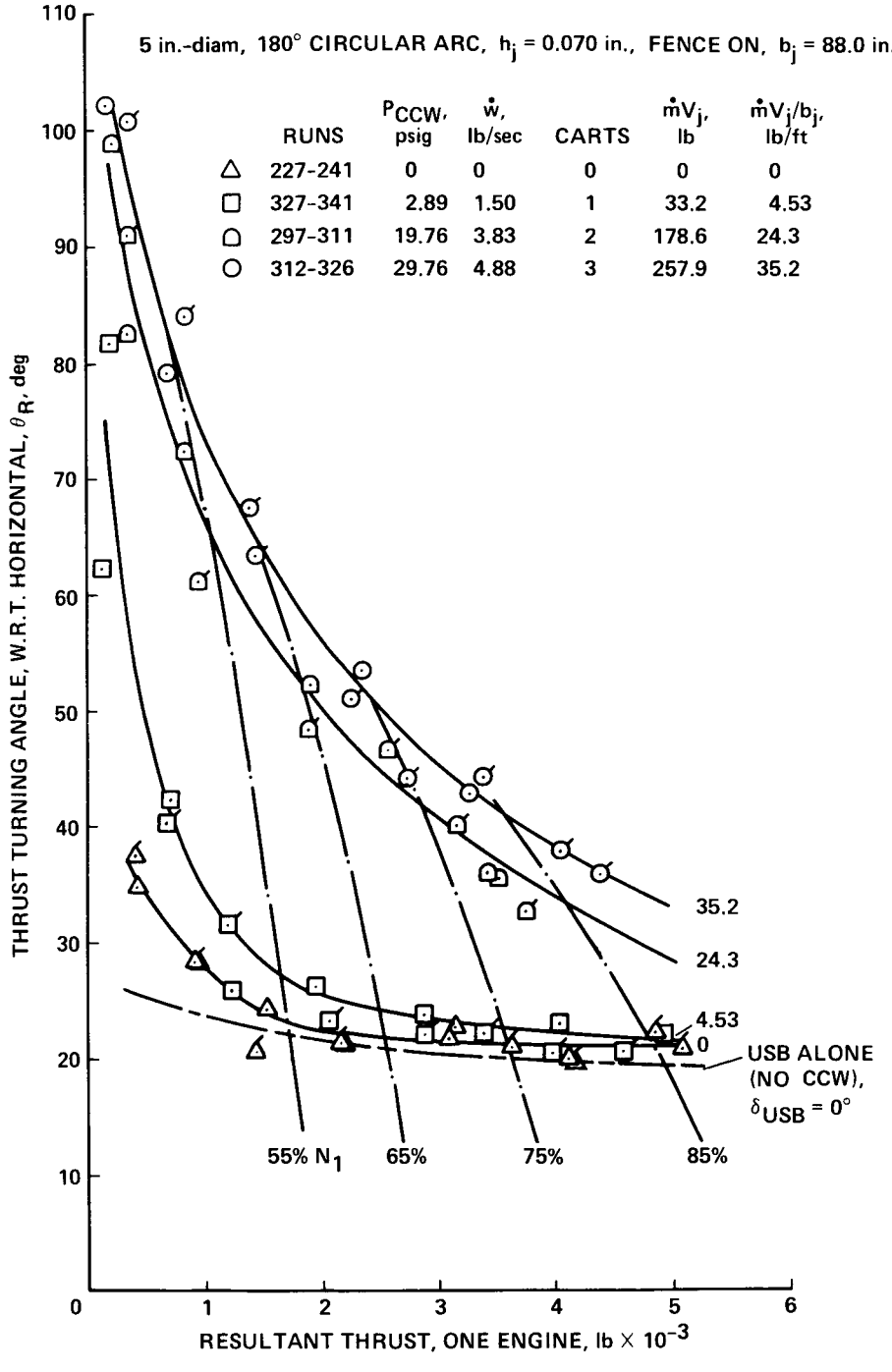


Figure 23.- Static thrust turning angle, configuration 5.

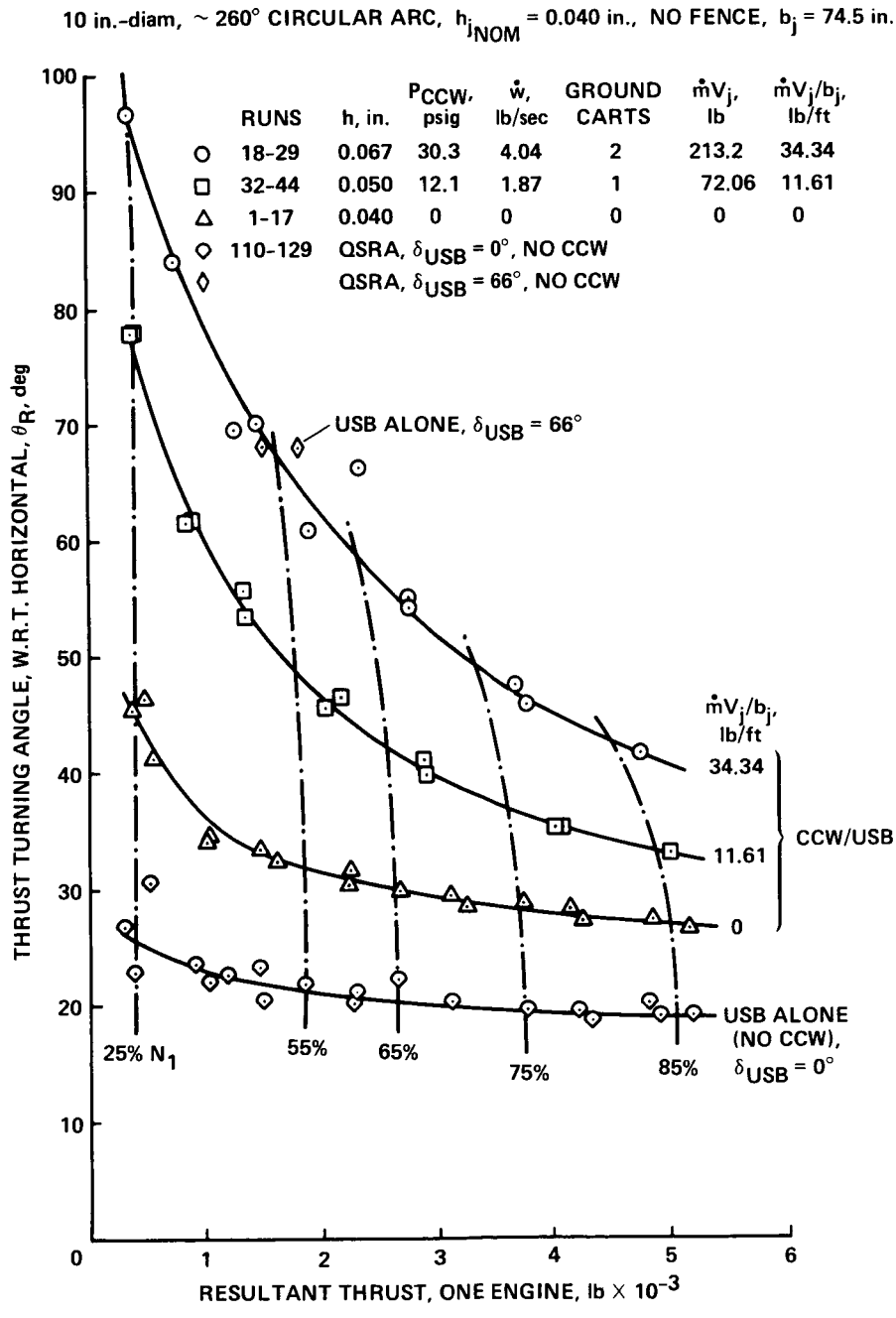


Figure 24.- Static thrust turning angle, Phase I baseline configuration (from NASA TM 84232).

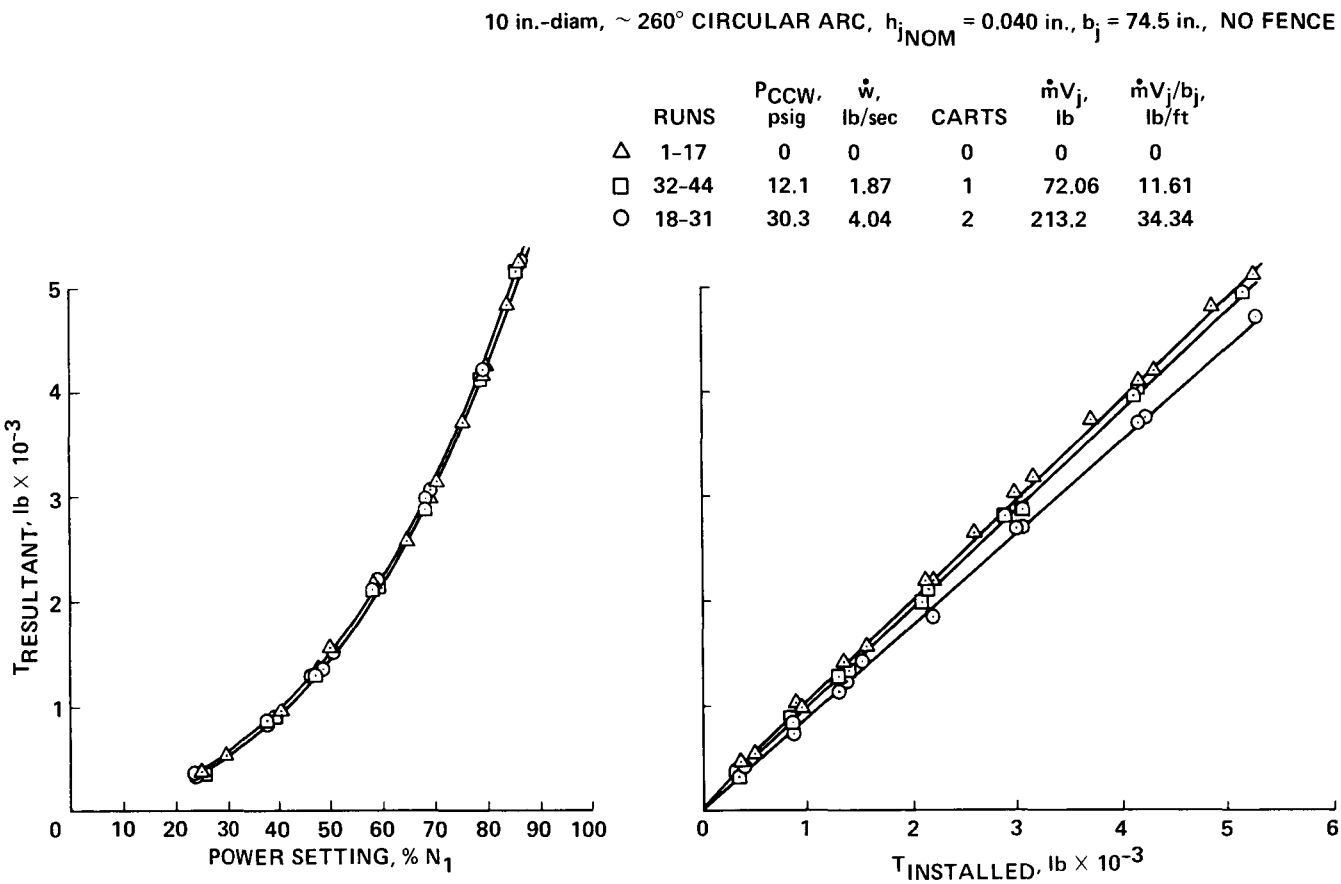


Figure 25.- Effect of blowing on resultant thrust, Phase I baseline configuration (from NASA TM 84232).

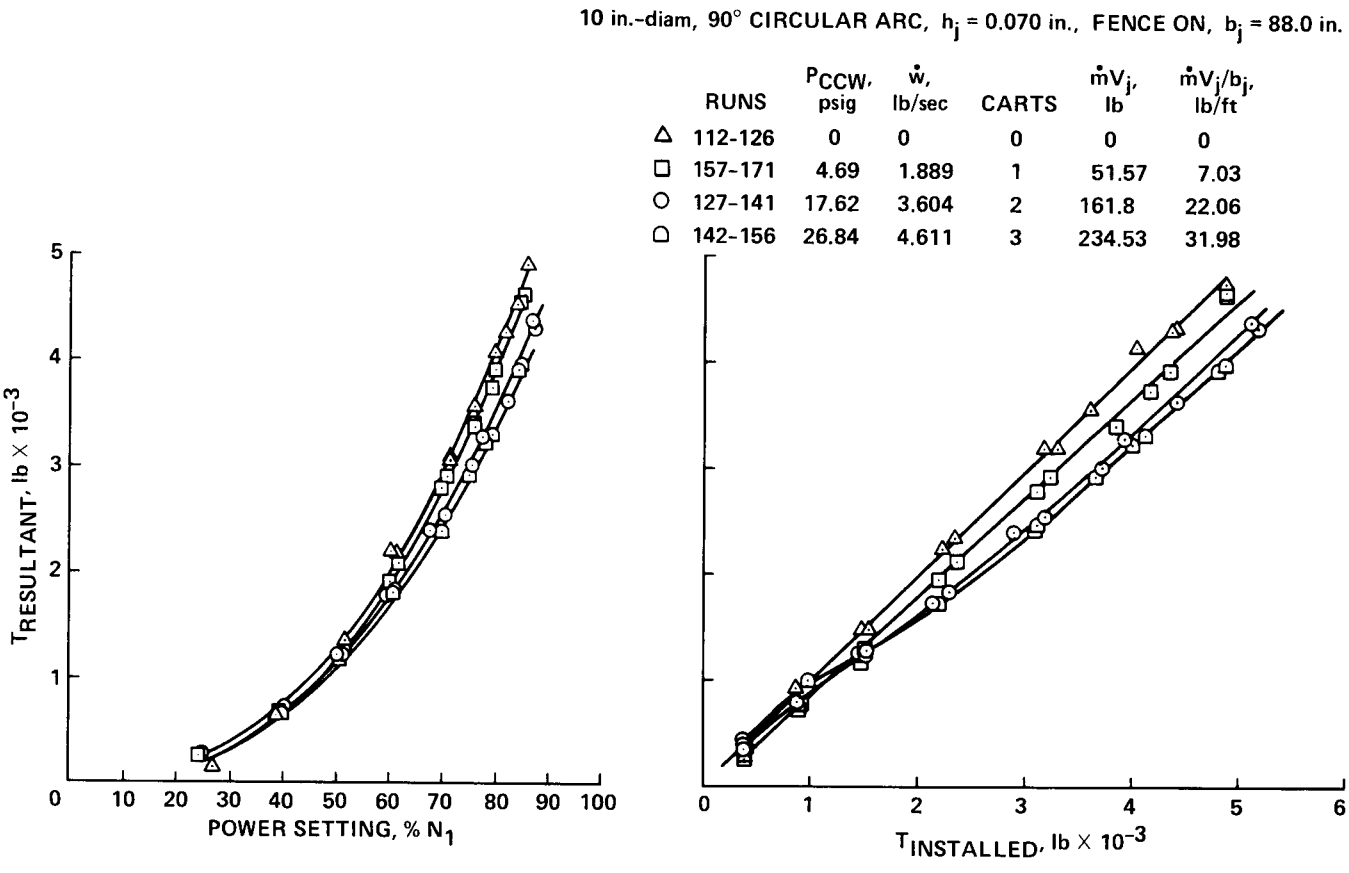


Figure 26.- Effect of blowing on resultant thrust, configuration 2.

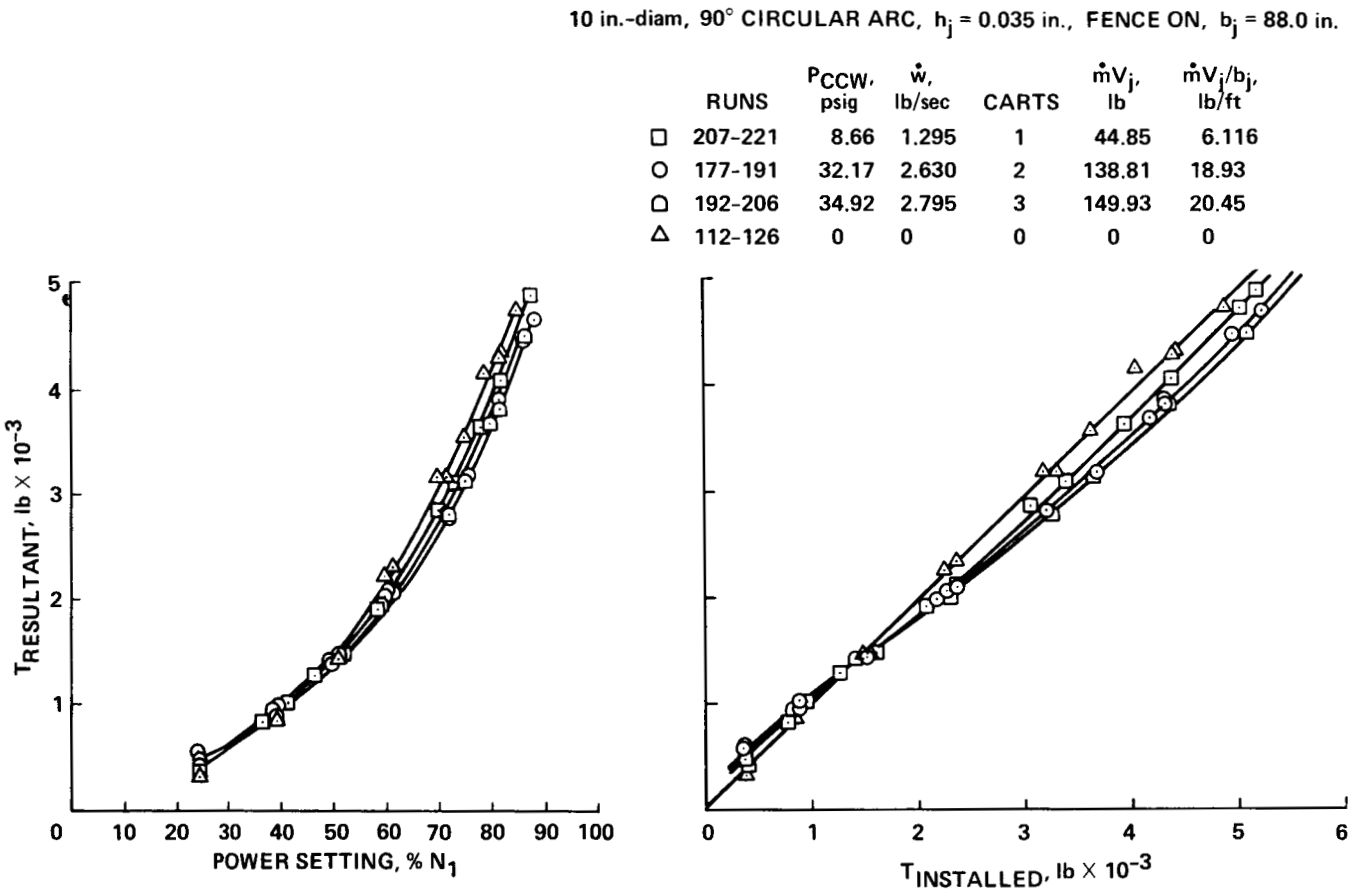


Figure 27.- Effect of blowing on resultant thrust, configuration 3.

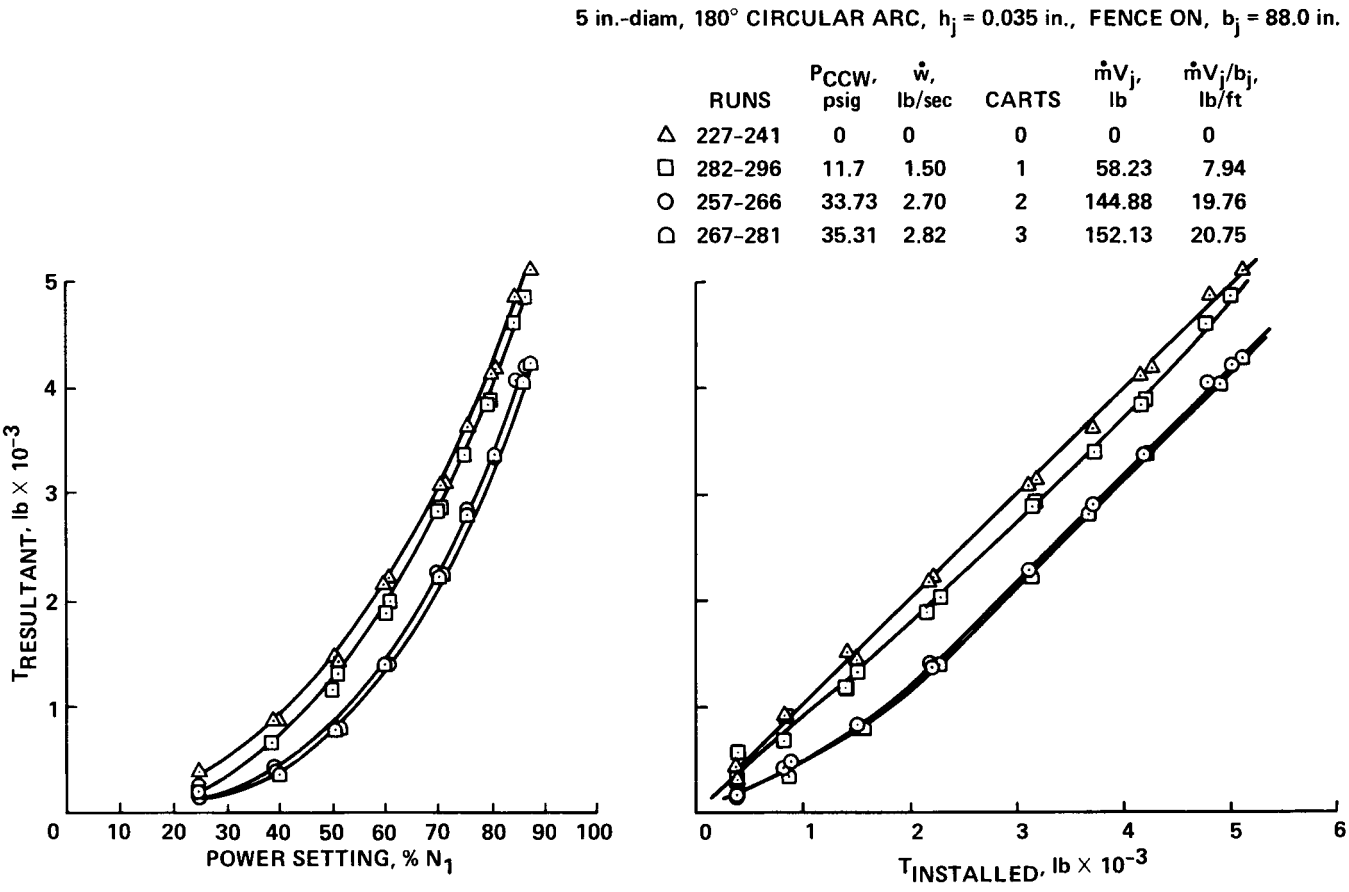


Figure 28.- Effect of blowing on resultant thrust, configuration 4.

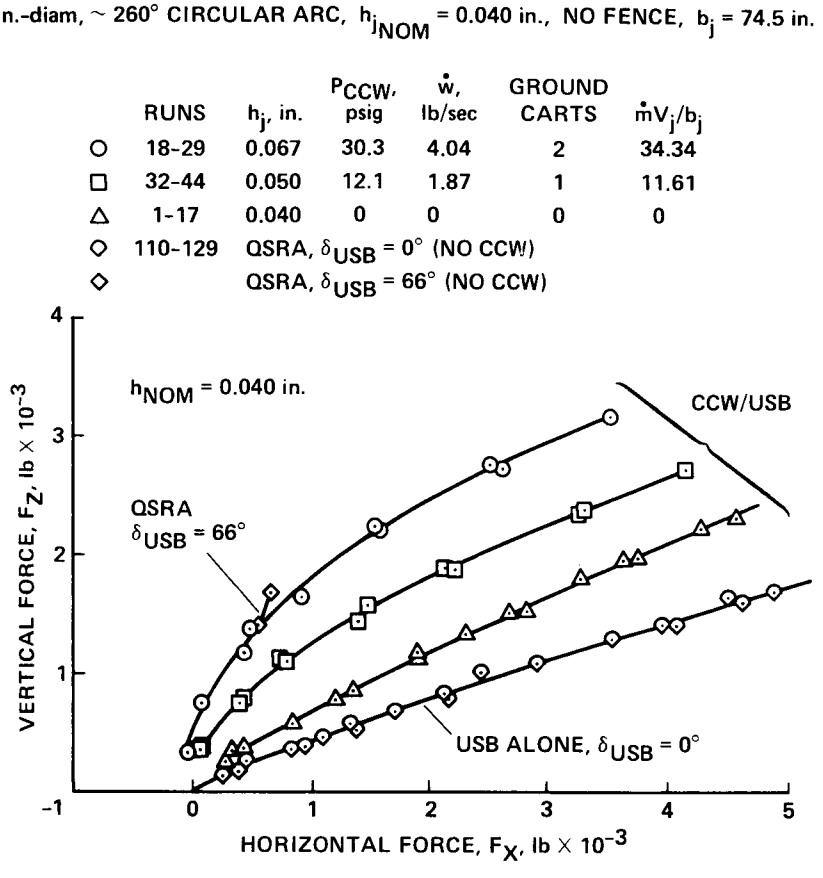


Figure 29.- Static thrust components, Phase I baseline configuration (from NASA TM 84232).

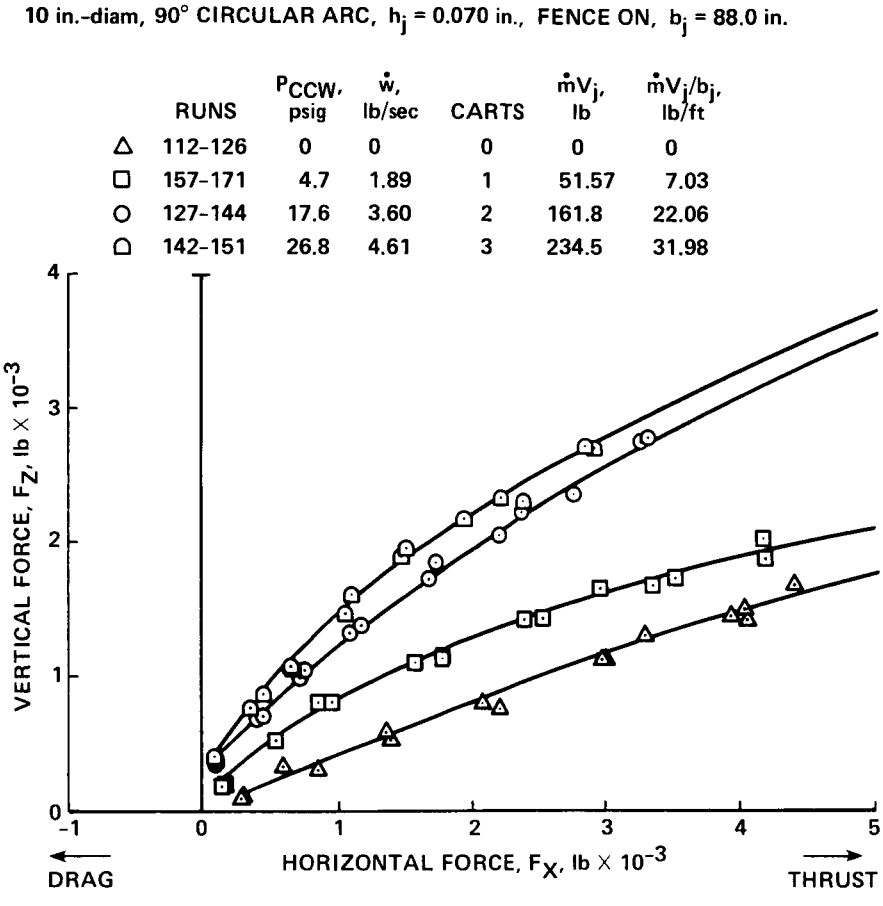


Figure 30.- Static thrust components, configuration 2.

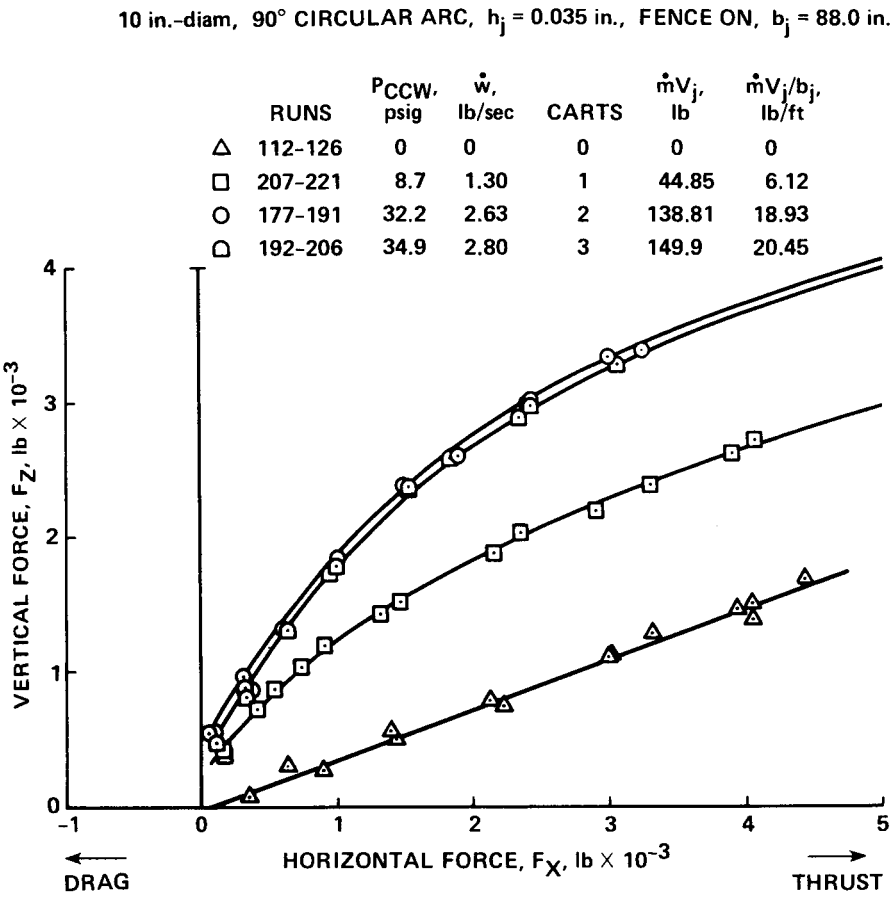


Figure 31.- Static thrust components, configuration 3.

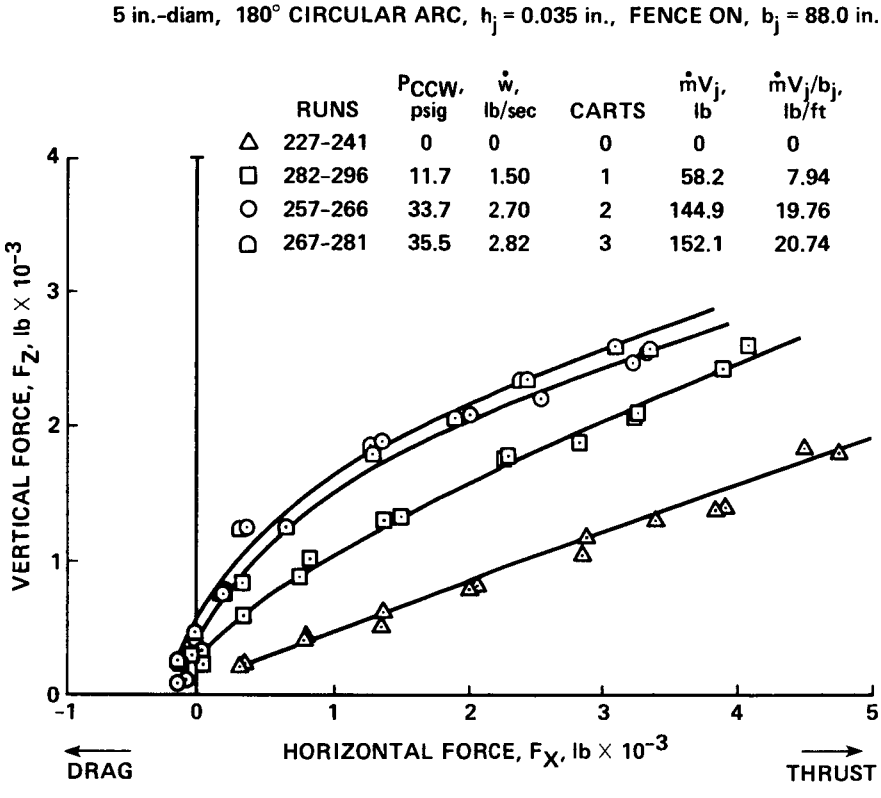


Figure 32.- Static thrust components, configuration 4.

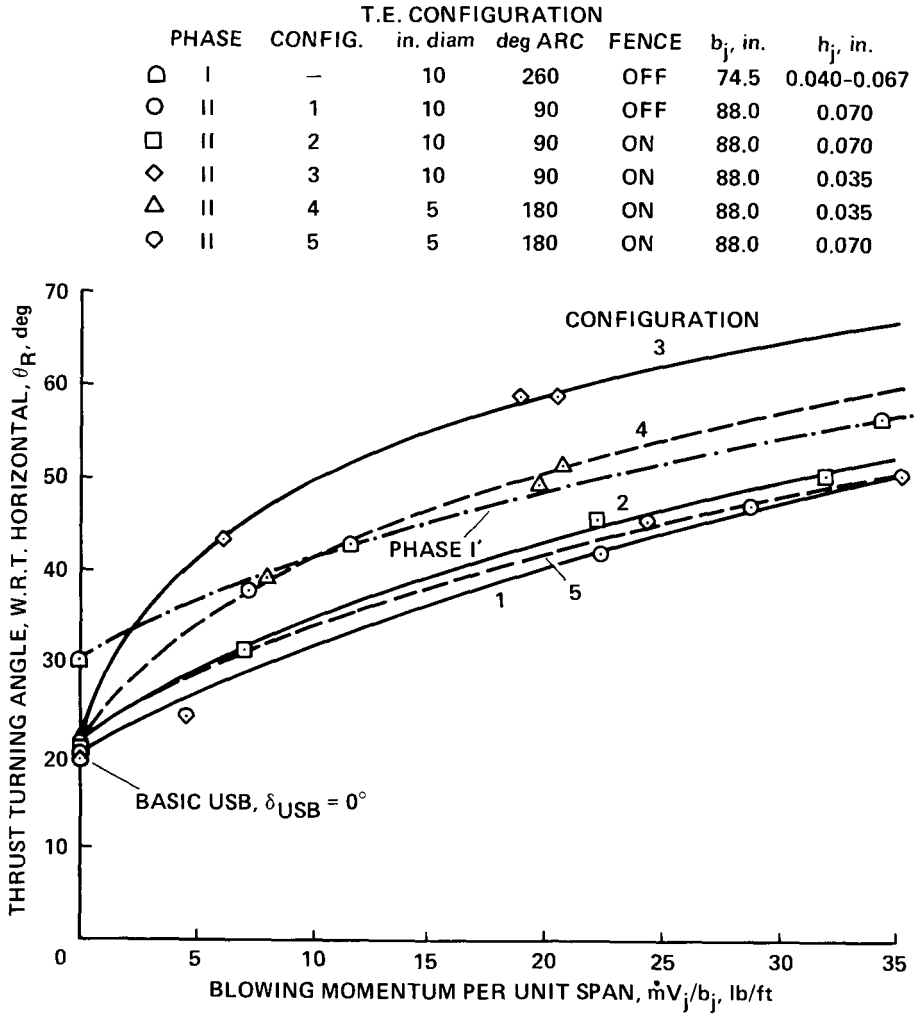


Figure 33.- Comparison of thrust deflection capability for a resultant thrust of 2500 lb (about half thrust).

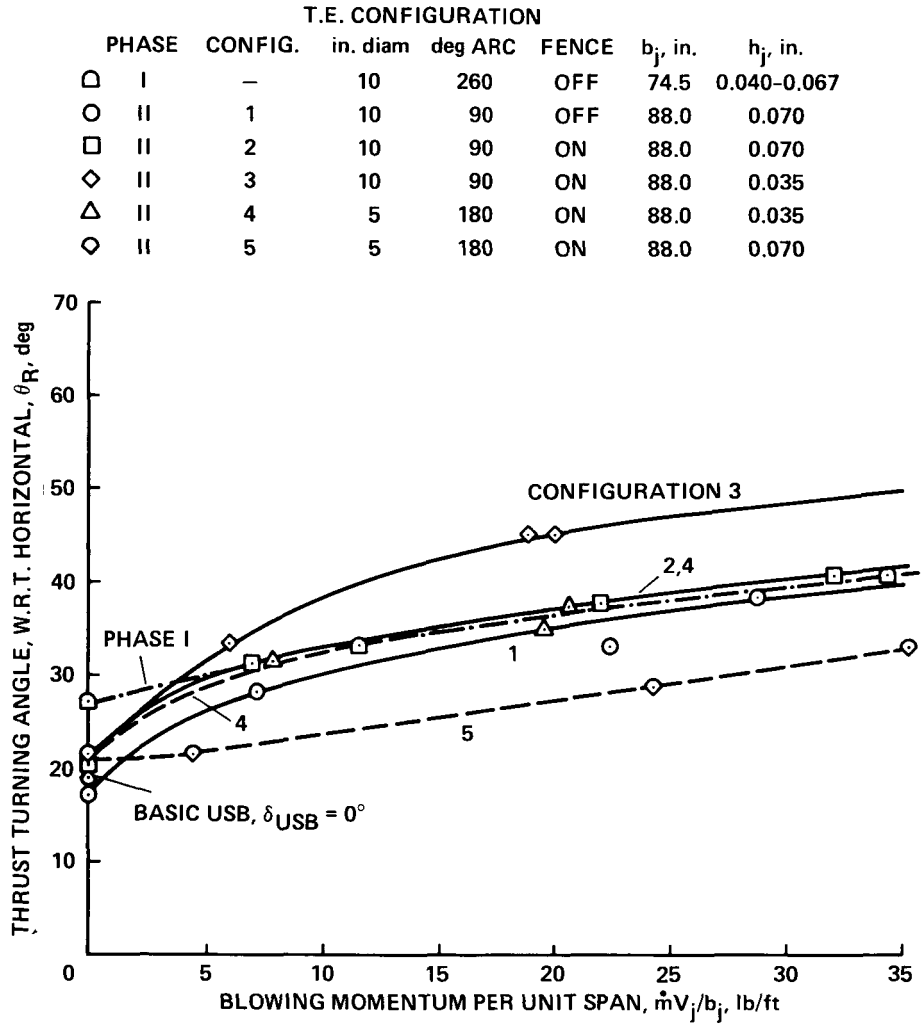


Figure 34.- Comparison of thrust deflection capability for a resultant thrust of 5000 lb (approximately full thrust).

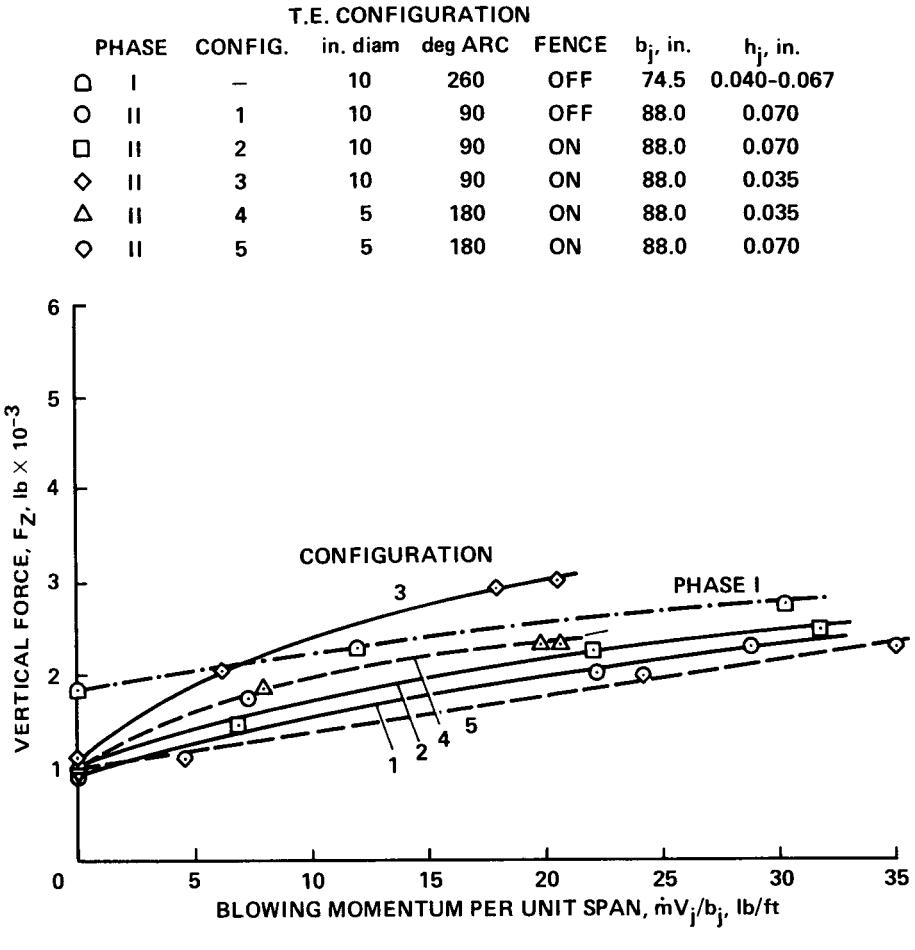


Figure 35.- Comparison of vertical force generation for a resultant thrust of 2500 lb (about half thrust).

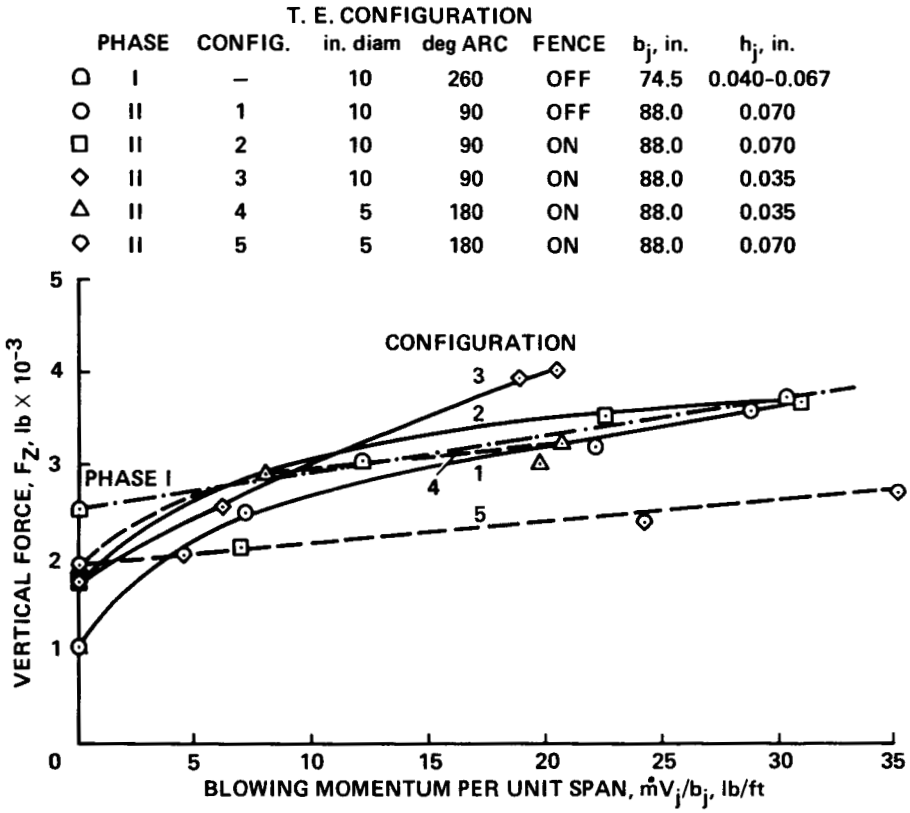


Figure 36.- Comparison of vertical force generation for a resultant thrust of 5000 lb (approximately full thrust).

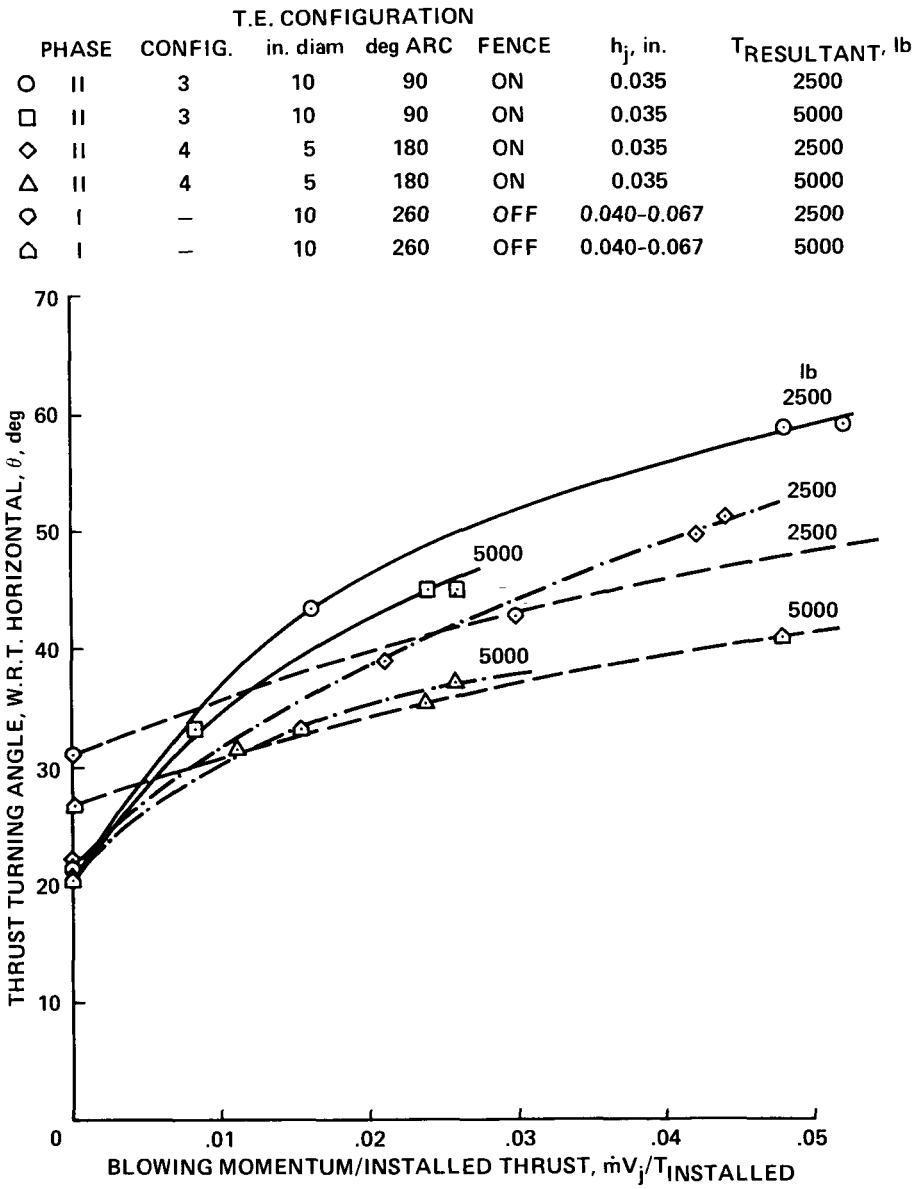


Figure 37.- Comparison of the CCW blowing momentum required for thrust turning.

| 1. Report No. | 2. Government Accession No. | 3. Recipient's Catalog No. |
|---|---|---|
| NASA TP-2684 | | |

| 4. Title and Subtitle | 5. Report Date |
|---|---|
| LARGE-SCALE STATIC INVESTIGATION OF CIRCULATION-CONTROL-WING CONCEPTS APPLIED TO UPPER-SURFACE-BLOWING AIRCRAFT | January 1987 |
| | 6. Performing Organization Code |
| 7. Author(s) | 8. Performing Organization Report No. |
| M. D. Shovlin, R. J. Englar, J. C. Eppel, and J. H. Nichols, Jr. | A-86117 |
| | 10. Work Unit No. |
| 9. Performing Organization Name and Address | 11. Contract or Grant No. |
| Ames Research Center<br>Moffett Field, CA 94035 | 13. Type of Report and Period Covered |
| 12. Sponsoring Agency Name and Address | Technical Paper |
| National Aeronautics and Space Administration<br>Washington, DC 20546 | 14. Sponsoring Agency Code |
| | 505-61-71 |

15. Supplementary Notes

Point of Contact: Michael D. Shovlin, Ames Research Center, MS 247-1, Moffett Field, CA 94035
(415) 694-6373 or FTS 464-6373

M. D. Shovlin and J. C. Eppel: Ames Research Center, Moffett Field, California.
R. J. Englar and J. H. Nichols, Jr.: David Taylor Naval Ship Research and Development Center, Bethesda, Maryland.

16. Abstract

The use of a circulation control to deflect turbofan engine thrust beyond 90° has been proven in full-scale static ground tests of the circulation-control-wing/upper-surface-blowing (CCW/USB) concept. This powered high-lift system employs a circular, blown trailing edge to replace the USB mechanical flaps to entrain engine-exhaust flow, and to obtain both a vertical-thrust component and an augmented circulation lift for short takeoff and landing (STOL) applications. Previous tests (Phase I), done in 1982, of a basic configuration installed on the Quiet Short Haul Research Aircraft confirmed these CCW/USB systems capabilities. A second phase (Phase II) of full-scale, static, thrust-deflection investigations has reconfirmed the ability to deflect engine thrust from 40° to 102°, depending on thrust level. Five new configurations were evaluated and performance improvements were noted for those configurations with larger blown span, fences or favorable engine interactions, smaller slot height, and larger radii with less than 180° of CCW surface arc. In general, a 90° circular arc with a smaller slot height provided the best performance, demonstrating that adequate thrust turning can be produced by a trailing-edge shape which may have minimal cruise-performance penalty. Thrust deflections were achieved at considerably lower blowing momentum than was required for the baseline case of Phase I. Improved performance and versatility were thus confirmed for the CCW/USB system applied to STOL aircraft, where the potential for developing a no-moving-parts pneumatic thrust deflector to rapidly vary horizontal force from thrust to drag, while maintaining constant vertical force, appears quite promising. The conversion from high-lift to lower-drag cruise mode by merely terminating the blowing provides an effective STOL aircraft system.

| 17. Key Words (Suggested by Author(s)) | 18. Distribution Statement |
|---|---|
| Circulation-control wing<br>Upper-surface blowing<br>Trust turning<br>Propulsive lift | Unclassified-Unlimited<br><br>Subject Category 05 |

| 19. Security Classif. (of this report) | 20. Security Classif. (of this page) | 21. No. of Pages | 22. Price* |
|---|---|---|---|
| Unclassified | Unclassified | 66 | A05 |

*For sale by the National Technical Information Service, Springfield, Virginia 22161

NASA-Langley, 1987